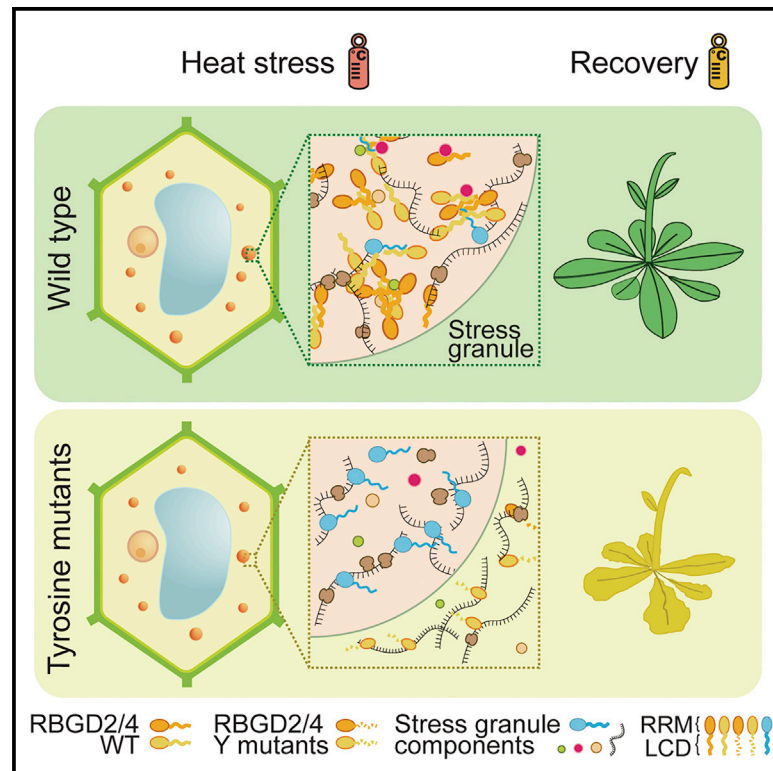


Developmental Cell

Liquid-liquid phase separation of RBGD2/4 is required for heat stress resistance in *Arabidopsis*

Graphical abstract



Authors

Shaobo Zhu, Jinge Gu,
Juanjuan Yao, ..., Dan Li, Heng Zhang,
Cong Liu

Correspondence

hengzhang@psc.ac.cn (H.Z.),
liulab@sioc.ac.cn (C.L.)

In brief

Zhu and Gu et al. discover two RNA binding proteins, RBGD2 and RBGD4, that phase separate in response to heat stress in plant cells and interact with specific heat-responsive transcripts. Their phase separation capacities, mediated by tyrosine residue arrays, are essential for their function in protecting plants from heat stress.

Highlights

- Two RNA binding proteins, RBGD2 and RBGD4, are required for heat stress in *Arabidopsis*
- Heat induces liquid-liquid phase separation (LLPS) of RBGD2/4 *in vitro* and *in vivo*
- Tyrosine residue arrays of RBGD2/4 are necessary for LLPS and plant heat resistance
- RBGD2/4 organize specific proteins and transcripts into stress granules

Article

Liquid-liquid phase separation of RBGD2/4 is required for heat stress resistance in *Arabidopsis*

Shaobo Zhu,^{1,2,7} Jinge Gu,^{2,3,7} Juanjuan Yao,^{1,2} Yichen Li,⁴ Zheting Zhang,^{1,2} Wencheng Xia,^{2,3} Zhen Wang,¹ Xinrui Gui,^{2,3} Leitong Li,¹ Dan Li,^{4,5} Heng Zhang,^{1,2,*} and Cong Liu^{3,6,8,*}

¹State Key Laboratory of Plant Molecular Genetics, Shanghai Center for Plant Stress Biology, CAS Center for Excellence in Molecular Plant Sciences, Chinese Academy of Sciences, Shanghai 200032, China

²University of Chinese Academy of Sciences, Beijing 100049, China

³Interdisciplinary Research Center on Biology and Chemistry, Shanghai Institute of Organic Chemistry, Chinese Academy of Sciences, Shanghai 201210, China

⁴Bio-X Institutes, Key Laboratory for the Genetics of Developmental and Neuropsychiatric Disorders, Ministry of Education, Shanghai Jiao Tong University, Shanghai 200030, China

⁵Zhangjiang Institute for Advanced Study, Shanghai Jiao Tong University, Shanghai 200240, China

⁶Department of Neurology and Institute of Neurology, Ruijin Hospital Affiliated to Shanghai Jiao Tong University School of Medicine, Shanghai 200025, China

⁷These authors contributed equally

⁸Lead contact

*Correspondence: hengzhang@psc.ac.cn (H.Z.), liulab@sioc.ac.cn (C.L.)

<https://doi.org/10.1016/j.devcel.2022.02.005>

SUMMARY

As sessile organisms, plants are highly sensitive to environmental stresses. In response to stresses, globally repressed translation initiation leads to stress granule (SG) formation. Protein liquid-liquid phase separation (LLPS) contributes to SG formation, but a direct link between protein LLPS and stress resistance has not yet been found in plants. Here, we report that two RNA-binding proteins, RBGD2 and RBGD4, function redundantly to improve heat resistance in *Arabidopsis*. RBGD2 and RBGD4 undergo LLPS *in vitro* and condense into heat-induced SGs *in vivo* via tyrosine residue array (TRA). Importantly, disrupting LLPS by mutating TRA abolishes RBGD2/4 condensation in SGs and impairs their protective function against heat stress (HS). Further study found that upon HS, the RBGD2/4 interaction network expands with additional SG proteins and heat-responsive mRNA. Our work shows a mechanistic basis that underlies protein LLPS in HS response in plants and suggests manipulation of protein LLPS as a general strategy to improve plant stress resistance.

INTRODUCTION

Temperature is an important environmental factor that affects the growth, development, and geographical distribution of plants. Excessively high temperature, or heat stress (HS), negatively affects plant growth and causes significant reduction in crop yield and quality (Ohama et al., 2017). High frequency of heat waves caused by global warming have devastating effects on agriculture worldwide (Battisti and Naylor, 2009). Understanding plant HS response is thus crucial for food security and developing heat-resistant crops. Previous studies demonstrated the essential role of transcriptional regulation in HS response for plant survival under HS (Ohama et al., 2017). A small family of heat-induced transcription factors HsfA1s (heat shock transcription factor A1s) function as the master regulators for both drought and HS response (Yoshida et al., 2011). Mutations in 3 of the 5 *HsfA1* genes (*hsfa1a/b/d*) severely compromised HS response and plant survival under HS (Liu et al.,

2011; Mishra et al., 2002; Yoshida et al., 2011). Through multiple transcriptional cascades, they activate the expression of HSPs (heat shock proteins) and ROS (reactive oxygen species)-scavenging enzymes that function in the defense of HS-induced protein unfolding and oxidative stresses.

In addition to transcriptional activation of the HS response cascade, HS also caused global translation inhibition, which induces the formation of stress granules (SGs), the membraneless organelle (MLO) composed of untranslating mRNAs, translation initiation factors (TIFs), RNA-binding proteins (RBPs), and other components (Chantarachot and Bailey-Serres, 2018; Gutierrez-Beltran et al., 2015; Lokdarshi et al., 2016; Sorenson and Bailey-Serres, 2014). The formation of SGs under various stress conditions has been commonly observed in many eukaryotes (Jain et al., 2016; Markmiller et al., 2018). Dysregulation of the dynamic assembly of human SGs is causative to various neurodegenerative diseases (Harrison and Shorter, 2017; Wolozin and Ivanov, 2019). In contrast, the function, composition, and

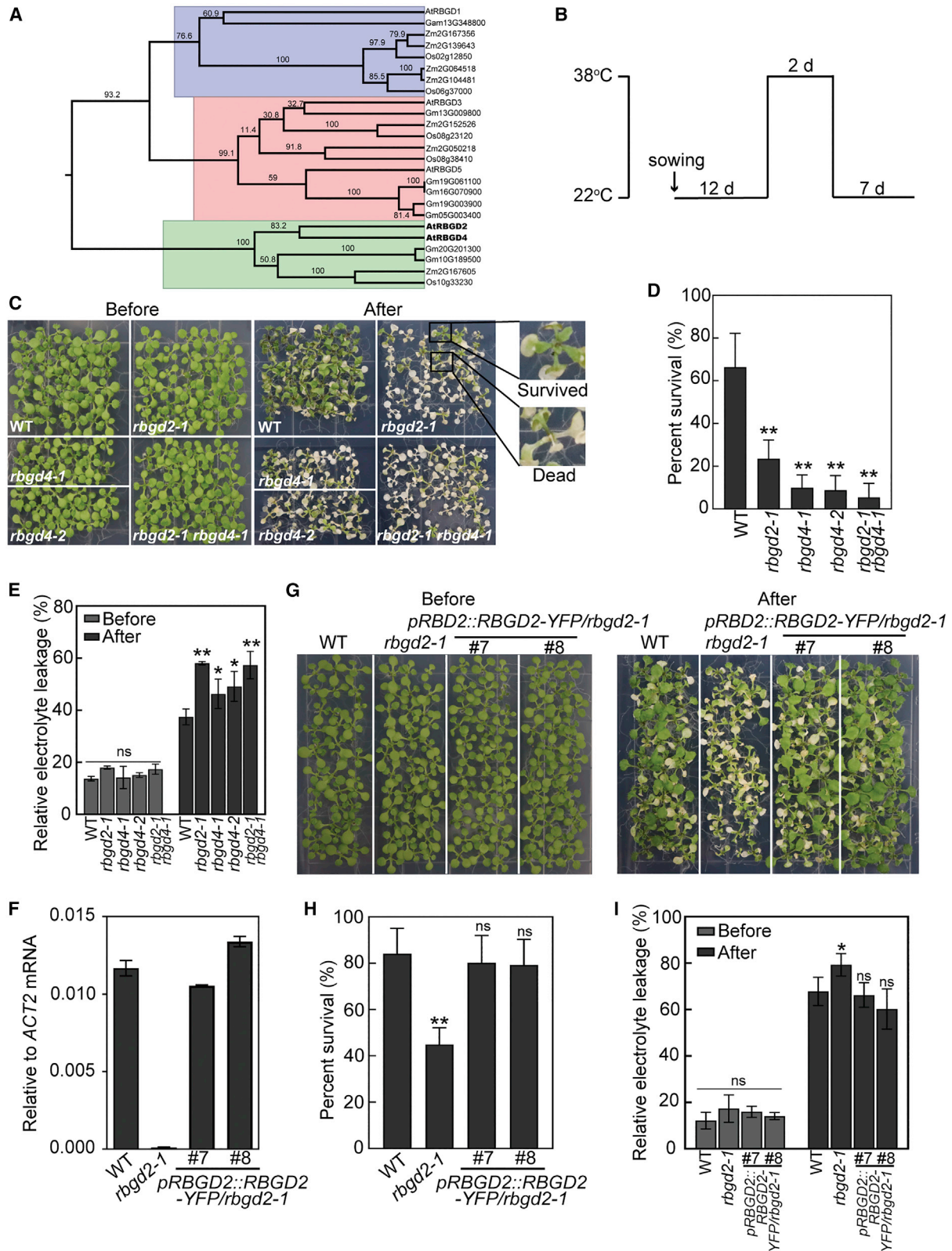


Figure 1. RBGD2 and RBGD4 promote heat resistance in Arabidopsis

(A) Phylogenetic analysis of plant RBGD proteins. Colored shades indicate the three major clades of RBGD proteins in plants. (B) Schematic diagram of heat treatment used in this experiment.

(legend continued on next page)

mechanism underlying the assembly of plant SGs are much less known. Several RBPs and TIFs, including PABs (poly(A)-binding proteins), Rbp47 (RNA-binding protein 47), UBP1 (oligouridylation binding protein 1), and eIFs (eukaryotic initiation factors), were used as SG markers in plants (Chantarachot and Bailey-Serres, 2018; Sorenson and Bailey-Serres, 2014; Weber et al., 2008) because their homologs were identified as SG components in yeast and mammalian cells (Jain et al., 2016). Previous studies showed that TSN1 (tudor staphylococcal nuclease 1) and TSN2 are colocalized with Rbp47b in the SGs and redundantly promote heat resistance in *Arabidopsis* (Gutierrez-Beltran et al., 2015). A recent study using mass-spectrometry-based approaches identified 118 proteins as components of the heat-induced SGs in *Arabidopsis*, including RBPs, metabolic enzymes, and signaling proteins (Kosmacz et al., 2019). About a quarter of these proteins are known or predicted SG components in yeast and mammalian cells (Kosmacz et al., 2019).

Liquid-liquid phase separation (LLPS) of proteins and RNAs are essential for the dynamic assembly of SGs (Molliex et al., 2015; Protter and Parker, 2016; Van Treeck et al., 2018). Several RBPs in mammals, e.g., fused in sarcoma (FUS), T-cell-restricted intracellular antigen-1 (TIA-1), and heterogeneous nuclear ribonucleoprotein A1 (hnRNP A1), were found to utilize their prion-like low-complexity domains (LCDs) to drive LLPS in mammalian SGs (Lin et al., 2015). Intriguingly, bioinformatics analyses identified hundreds of proteins that contain prion-like domains in *Arabidopsis* (Chakrabortee et al., 2016), implying that protein LLPS is also critical for the formation of different MLOs in plants. Recently, several plant proteins were found to undergo LLPS and are involved in MLO formation during different biological processes, e.g., LLPS of Rubisco-CcmM network in β -carboxysome biogenesis (Wang et al., 2019); co-LLPS of Rubisco and essential pyrenoid component 1 (EPYC1) in the pyrenoid, an carbon-fixing MLO in certain algae (Freeman Rosenzweig et al., 2017); co-LLPS of FLL2 and flowering control locus A (FCA) in the FCA nuclear body, and both proteins are required for the alternative polyadenylation of the flowering repressor gene *flowering control locus C* (*FLC*) (Fang et al., 2019); and co-LLPS of H3K9me3 nucleosome arrays and Agenet domain-containing P1 (ADCP1/AGDP1), an Agenet-domain containing protein that is required for heterochromatic chromocenter formation and DNA methylation (Zhang et al., 2018; Zhao et al., 2019). In contrast, although multiple SG components are required for plant stress resistance, whether they undergo LLPS and how protein LLPS is involved in SG function and stress response remain poorly understood.

RBPs are highly enriched in SG proteins (Jain et al., 2016; Markmiller et al., 2018) and accumulating evidences show that RBPs play essential roles in plant stress resistance (Ambrosone

et al., 2012; Nakaminami et al., 2012). RBPs also display the potential to elevate stress tolerance of cells via condensation (Riback et al., 2017). We thus mainly focused on the RBPs with LCD in this study, and we discovered two RBPs named RBGD2 and RBGD4 (RNA-binding glycine-rich D2 and D4) as components of the heat-induced SGs. RBGD2 and RBGD4 form highly dynamic granule-like structures colocalized with SG markers in the cell and are essential for heat resistance in *Arabidopsis*. Both RBGD2 and RBGD4 contain LCDs that exhibit high capability for LLPS *in vitro*. We further identified that the tyrosine residue array (TRA) in the LCDs of RBGD2/4 is responsible for driving their LLPS, which is necessary for their function in heat resistance. HS promotes the formation of a RBGD2/4-containing protein-protein interaction (PPI) network and the recruitment of a number of heat-responsive transcripts into the SGs. Our work provides the mechanistic basis underlying RBGD2/4 LLPS and identifies a direct link between LLPS of RBPs and heat resistance in plants.

RESULTS

RBGD2/4 play an important role in resistance of HS in plants

While searching for RBPs that function in plant abiotic stress response, we identified two *RBGD* (RNA-binding glycine-rich group D) genes in *Arabidopsis thaliana* whose expression levels are significantly elevated upon HS. Quantitative reverse transcriptase PCR (qRT-PCR) indicated that the transcripts of the *RBGD2* and *RBGD4* were upregulated by 2-fold to 4-fold within 30 min and persisted up to 10 h after heat treatment (Figure S1A). The *Arabidopsis* genome contains 5 *RBGD* genes, one on each chromosome. Phylogenetic analyses of plant *RBGD* proteins identified three major clades in plants (Figure 1A). *RBGD2* and *RBGD4* belong to the same clade, suggesting that they are functionally similar (Figure 1A). Expression analyses of *RBGD2/4* in different *Arabidopsis* tissues demonstrated that these two genes are ubiquitously expressed in most organs except for roots, with significantly higher expression in leaves and seeds (Figure S1B).

To investigate the function of *RBGD2* and *RBGD4* in plant heat response, we examined the phenotype in loss-of-function mutants of the two genes. We ordered 2 T-DNA lines for each gene from the *Arabidopsis* Biological Resource Center (ABRC). PCR-based genotyping identified the homozygous mutants, but further sequencing of the T-DNA border sequences indicated that the two mutants for *RBGD2* (SALK_202494 and SALK_040839) are the same allele (Figures S1C and S1D). The qRT-PCR analyses indicated that the T-DNA insertion in *rbgd2-1* abolished the expression of *RBGD2*, whereas the expression of *RBGD4* in the two mutant alleles (*rbgd4-1* and *rbgd4-2*)

(C) Images of single mutants (*rbgd2-1*, *rbgd4-1*, and *rbgd4-2*) and double mutant (*rbgd2 rbgd4*) seedlings that were subject to heat shock treatment as indicated in (B). Enlarged images showing representative dead and live seedlings after the heat treatment and recovery growth.

(D) Calculated survival rates of mutant seedlings after heat treatment. Data are presented as mean \pm SD, $n = 3$.

(E) Relative electrolyte leakage of mutant seedlings after 2-day heat treatment. Data are presented as mean \pm SD. $n = 3$.

(F) Quantified transcript levels of the *RBGD2-YFP* transgene. The transcript level is calculated relative to *ACT2*; error bars represent the \pm SD of triplicate reactions.

(G) Images of *pRBGD2::RBGD2-YFP/rbgd2* plants seedlings that were subject to heat treatment as indicated in (B).

(H) Calculated survival rates of *pRBGD2::RBGD2-YFP/rbgd2* plants after heat treatment. Data are presented as mean \pm SD, $n = 3$.

(I) Relative electrolyte leakage of *RBGD2* complementation lines. Data are presented as mean \pm SD. $n = 3$.

Statistically significant differences with respect to the control (WT) are indicated as: * $p < 0.05$ and ** $p < 0.01$. See also Figure S1.

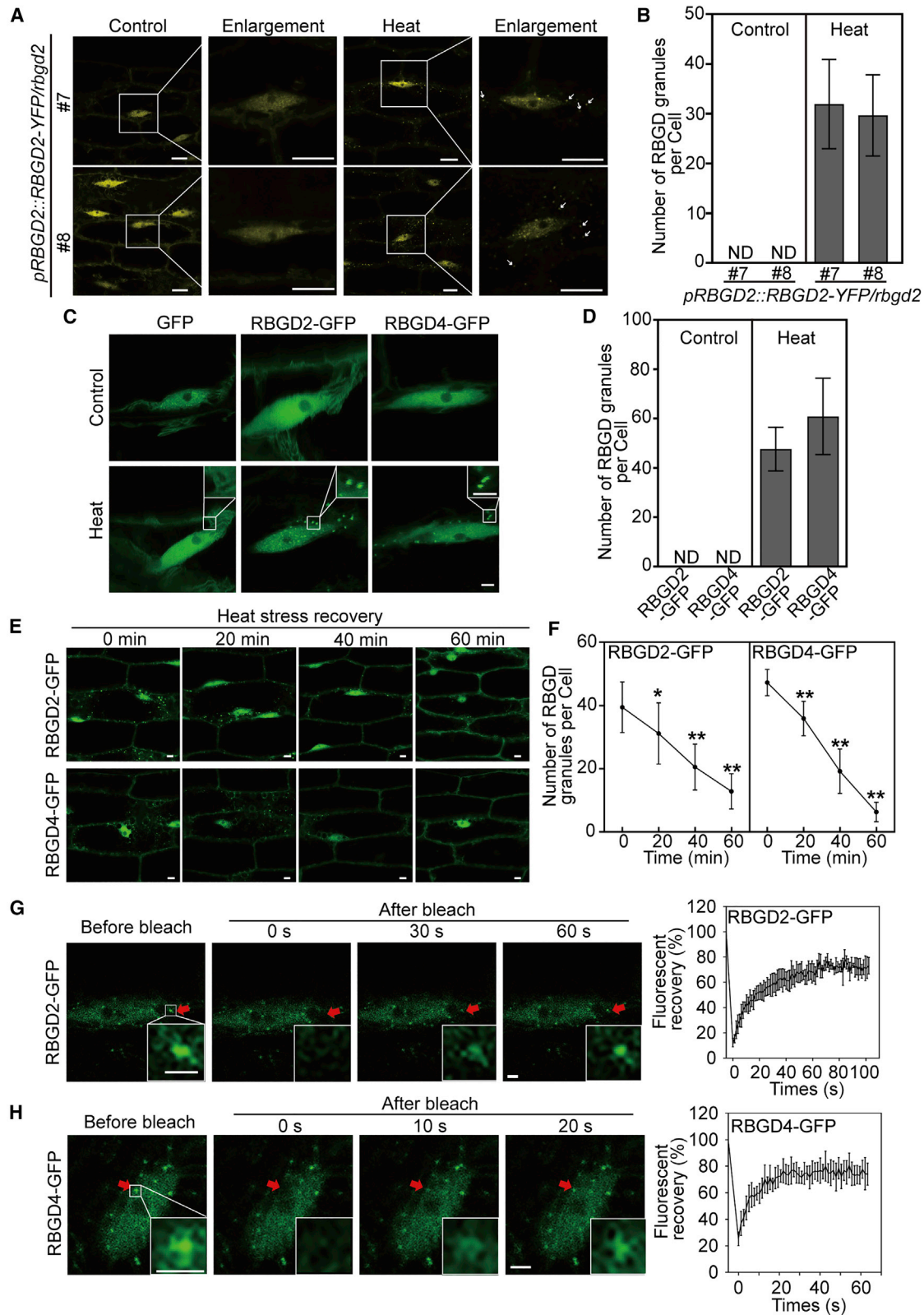


Figure 2. RBGD2/4 form dynamic granule-like structures *in vivo* in response to HS

(A) Native promoter-driven RBGD2-YFP proteins form granule-like structures (white arrows indicate representative granule-like structures) after heat treatment. Scale bars, 10 μ m.

(legend continued on next page)

decreased to ~25% of the wild-type (WT) level (Figure S1E). The *rbgd2-1 rbgd4-1* double mutant was generated through crossing. Neither single mutants nor the double mutant exhibited visible abnormalities during the whole life cycle under normal growth conditions. We subjected seedlings to long-term mild HS (2 days at 38°C) or short-term strong HS treatment (4.5 h at 42°C), and then let them recover at normal temperature (22°C) for 7–10 days (Figures 1B and S1F). All the mutant seedlings, including *rbgd2-1*, *rbgd4-1*, *rbgd4-2*, and *rbgd2-1 rbgd4-1*, exhibit significantly lower survival rates compared with the WT control under different heat treatments (Figures 1C, 1D, S1G, and S1H). Consistent with the recovered growth phenotype, we found that mutants of *rbgd2* and/or *rbgd4* exhibited higher electrolyte leakage compared with WT seedlings after heat treatment, indicating that the membrane integrity is more affected in these mutants (Figure 1E). We next generated native promoter-driven *RBGD2-YFP* (*pRBGD2::RBGD2-YFP*) transgenic plants in the *rbgd2-1* background. The qRT-PCR analysis showed that the *RBGD2-YFP* mRNA was expressed at similar levels of the *RBGD2* mRNA in WT plants (Figure 1F). The reduced survival rate and enhanced electrolyte leakage phenotype of *rbgd2-1* after heat treatment were also restored to WT levels by the *pRBGD2::RBGD2-YFP* transgene (Figures 1G–1I). We also examined the phenotype of *RBGD2* and *RBGD4* overexpressing plants after HS. The *35S::RBGD2-GFP* and *35S::RBGD4-GFP* seedlings exhibited 6-fold to 26-fold higher expression levels of *RBGD2* or *RBGD4* than WT and had significantly higher survival rates compared with the WT control after stress treatment (Figures S1F and S1I–S1L). These results indicate that *RBGD2* and *RBGD4* are essential for HS resistance in *Arabidopsis*.

RBGD2/4 form granule-like structures in cells upon HS

We next sought to investigate the underlying mechanism of how *RBGD2* and *RBGD4* enhance plant heat resistance. We used *pRBGD2::RBGD2-YFP* transgenic plants (Figure 1F) in the *rbgd2-1* background to examine the subcellular localization of *RBGD2-YFP* under the confocal fluorescence microscope before and after heat treatment (Figures 2A and 2B). Most *RBGD2* signals were polydisperse in both the cytosol and the nucleus under normal conditions but spontaneously formed a plenty of granule-like structures within 30 min of heat treatment (Figures 2A and 2B). The subcellular localization of *RBGD2* and *RBGD4* proteins in the overexpression lines (*35S::RBGD2-GFP* and *35S::RBGD4-GFP*) exhibited similar patterns. Both *RBGD2-GFP* and *RBGD4-GFP* spontaneously formed granule-like structures within 30 min of heat treatment (Figures 2C, 2D,

S2A, and S2B). Anti-GFP western blots indicated that the level of *RBGD2/4-GFP* proteins remained constant before and after heat treatment (Figure S2C). To further rule out the possibility that puncta formation was triggered by GFP dimerization, we prepared the monomeric version of both GFP and red fluorescent protein (RFP). The *RBGD2/4* fused with monomeric versions of the fluorescent proteins still formed heat-induced *RBGD2/4* granules (Figure S2D).

Moreover, the formation of *RBGD*-containing granules is reversible in cells. Placing the heat-treated seedlings back to normal growth temperature for 60 min significantly reduced the number of granules in the cell (Figures 2E and 2F), indicating that the heat-induced granule-like structure is dynamically regulated *in vivo*. We further examined the dynamics of *RBGD*-containing granules using FRAP (fluorescence recovery after photo-bleaching). We found that the fluorescent intensity of *RBGD2*- and *RBGD4*-containing granules rapidly recovered within 20–50 s after photobleaching, indicating that these structures are highly dynamic (Figures 2G and 2H).

We also examined the subcellular localization of *RBGD2* and *RBGD4* proteins under other types of abiotic stress. *RBGD2*- or *RBGD4*-containing granules were not observed in plant cells up to 2.5 h of cold (4°C), salt (125 mM NaCl), or osmotic (300 mM mannitol) stress treatment, indicating that the formation of *RBGD2/4* granules was not a common phenomenon under different stress (Figure S2E).

Since phylogenetic and genetic analyses indicated that *RBGD2* and *RBGD4* may function redundantly, we further tested the possibility that the two proteins are localized to the same granule-like structures. Transient expression of *RBGD2-GFP* and *RBGD4-RFP* in *Arabidopsis* protoplasts indeed identified that the majority of GFP and RFP signals overlapped and formed granule-like structures after heat treatment (Figure S2F). Thus, in response to HS, *RBGD2* and *RBGD4* are condensed into the same granule-like structures in plant cells.

RBGD2/4 undergo LLPS *in vitro*

We next asked whether *RBGD2/4* themselves are capable of undergoing LLPS *in vitro*. Recombinant full-length (FL) *RBGD2* and *RBGD4* were individually expressed in *E. coli* and purified to high homogeneity. *RBGD2/4* displayed high phase separation ability and formed spherical droplets under various conditions, including low salt concentration, polyarginine (peptide CR₂₀), and crowding reagents (dextran, ficoll, or polyethylene glycol [PEG]) that mimic the crowding environment in the cell (Wegmann et al., 2018; Figures 3A and S3A). Under those conditions,

(B) Quantification of the number of *RBGD* granules per cell under control and heat conditions in (A). Data are presented as mean ± SD. *pRBGD2::RBGD2-YFP/rbgd2-1* (#7 [n = 30], #8 [n = 30]). ND, not detected.

(C) Subcellular localization of *RBGD2-GFP* and *RBGD4-GFP* before and after 30-min heat treatment. Transgenic GFP protein was used as a negative control. Scale bars: 2 and 1 μm (zoom in).

(D) Quantification of the number of *RBGD* granules per cell under control and heat conditions in (C). Data are presented as mean ± SD. *RBGD2-GFP* (n = 30) and *RBGD4-GFP* (n = 30). ND, not detected.

(E) Subcellular localization of *RBGD2/4-GFP* during HS recovery. Scale bars, 5 μm.

(F) Quantification of the number of *RBGD* granules per cell using images in (E). Each time point: n = 20. Data are presented as mean ± SD. Statistically significant differences with respect to the 0 time are indicated as: *p < 0.05 and **p < 0.01.

(G and H) Images and quantification of FRAP of *RBGD2*- (G) and *RBGD4*-containing (H) granules, respectively. The images shown are representative of 6 (*RBGD2-GFP*) and 8 (*RBGD4-GFP*) independent observations. Plots on the right indicate quantified fluorescent signals over the time course after photobleaching. Data are presented as mean ± SD. Scale bars: 2, 1 (G zoom in), and 0.5 μm (H zoom in).

See also Figure S2.

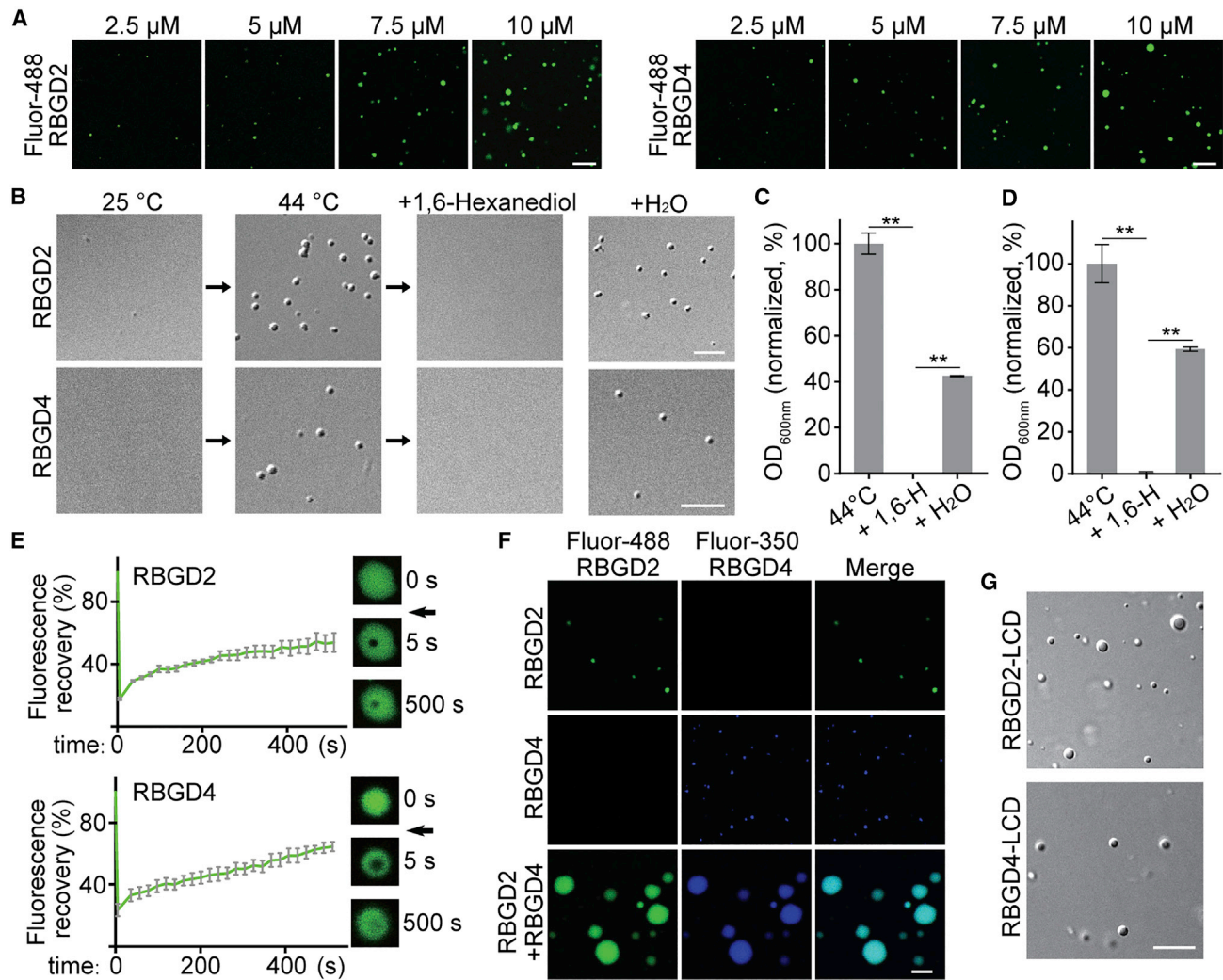


Figure 3. RBGD2 and RBGD4 proteins undergo LLPS *in vitro*

(A) LLPS of purified RBGD2 and RBGD4 proteins under micromolar protein concentrations. LLPS condition: 100 mM NaCl, pH 7.5 and 15% PEG 8,000. Scale bars, 5 μ m.

(B) Representative DIC images showing droplet formation of 20 μ M RBGD2/4 proteins as temperature increases from 25°C to 44°C under 100 mM NaCl and pH 7.5. Addition of 1 volume of 30% 1,6-hexanediol solution disrupts RBGD2/4 phase separation, but not the solvent (water). Scale bars, 5 μ m.

(C and D) Turbidity measurement of RBGD2 (C) and RBGD4 (D) solutions shown in (B). Data are presented as mean \pm SEM, n = 3. **p < 0.01.

(E) RBGD2/4 *in vitro* droplets display liquid-like property. FRAP curves of RBGD2/4 and representative droplets before and after photobleaching; the black arrows indicate time of photobleaching. Data are presented as mean \pm SEM, n = 4.

(F) Co-LLPS of RBGD2 and RBGD4 *in vitro*. LLPS was performed with 30 μ M RBGD2 and/or 25 μ M RBGD4, 150 mM NaCl, pH 7.5, and 15% dextran 70. Scale bars, 5 μ m.

(G) The LCD is sufficient for LLPS. LLPS of 50 μ M purified LCDs of RBGD2/4 in the presence of 150 mM NaCl, pH 7.5, and 15% dextran 70. Scale bars, 5 μ m.

See also Figure S3.

RBGD2/4 were even observed to form droplets at a protein concentration as low as 2.5 μ M (Figure 3A). Remarkably, temperature change could also trigger RBGD2/4 phase separation (Figures 3B and S3A). Consistent with the observation that RBGD2/4 form granule-like structures under HS in cells (Figure 2), increasing temperature from 25°C to 44°C induced the phase separation of RBGD2/4 *in vitro* (Figures 3B, S3B, and S3C). The heat-induced droplets cannot totally disappear with the decrease in temperature (Figures S3B and S3C). However, addi-

tion of 1,6-hexanediol, which disrupts hydrophobic interactions, can totally dissolve those droplets (Figures 3B–3D; Krainer et al., 2021). We further performed FRAP experiments to probe the mobility of RBGD2/4 within the droplets. The FRAP results showed that the intensity of the Fluor-488-labeled RBGD2/4 fluorescence signal recovered partially after photobleaching (Figures 3E and S3D). More interestingly, RBGD2 and RBGD4 could cophase separate when mixed together *in vitro* (Figure 3F). This observation is in line with our observation that RBGD2 and

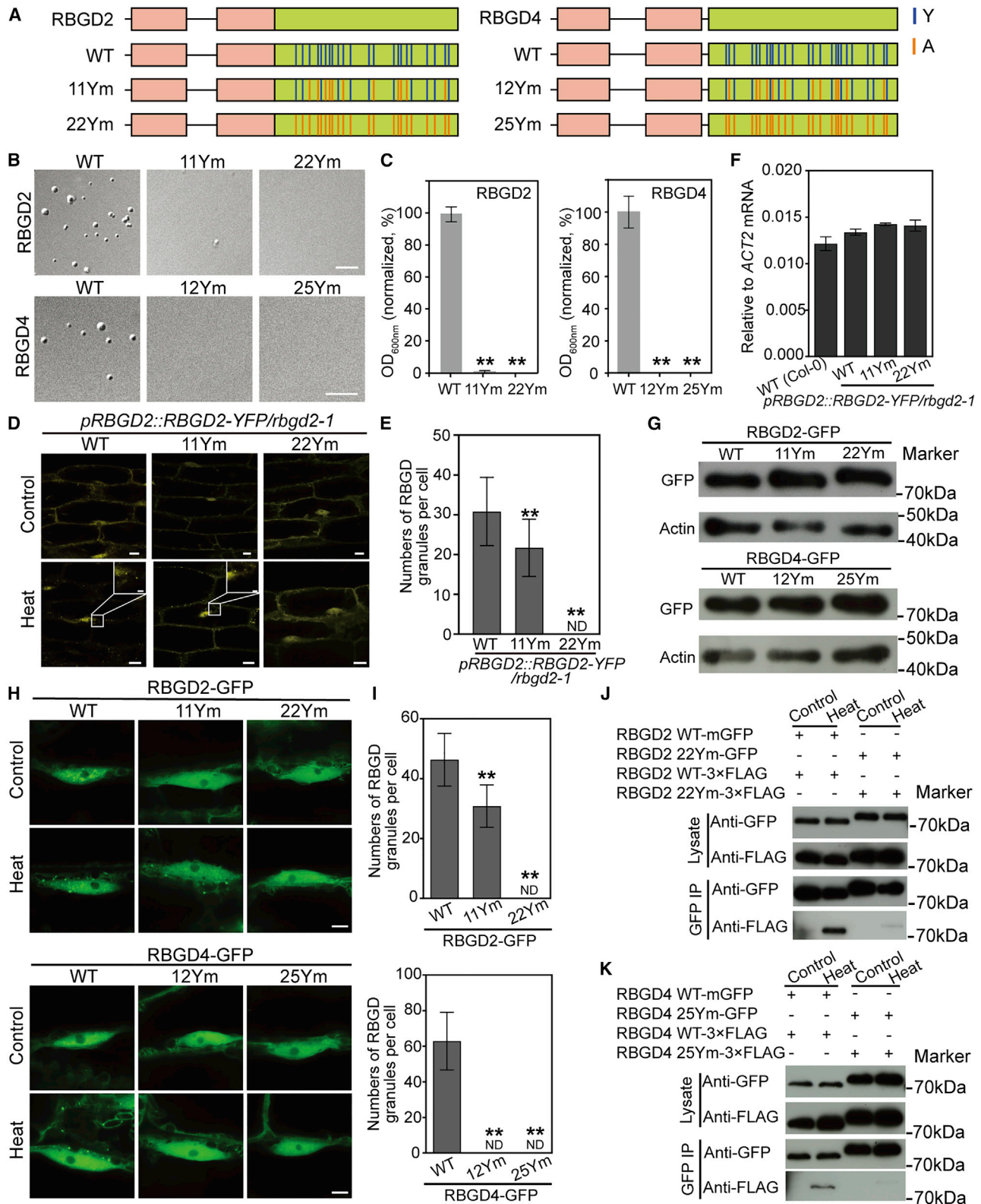


Figure 4. Tyr residues in the LCD are responsible for mediating LLPS both *in vitro* and *in vivo*

(A) Domain architecture of the RBGD2 and RBGD4 protein. Coral and green boxes each represent the RRM (RNA recognition motif) domain and the LCD (low-complexity domain). Blue lines indicate the positions of Tyr residues in the LCD, and orange lines indicate Tyr residues mutated to Ala.

(legend continued on next page)

RBGD4 were condensed into the same heat-induced granules *in vivo* (Figure S2F). Together, these results demonstrate that both RBGD2 and RBGD4 exhibit high tendency to undergo phase separation, and they can phase separate on their own or cophase separate *in vitro*.

Mechanistic basis underlying the LLPS of RBGD2/4

To decipher the molecular mechanism of LLPS in RBGD2/4, we analyzed the primary sequences of RBGD2 and RBGD4. As members of the RBGD family, both RBGD2 and RBGD4 contain two well-folded RRM (RNA recognition motif) domains in the N terminus and an LCD in the C terminus (Figures S3E and S3F). Since LCD is implicated in several proteins as the key feature to mediate protein LLPS (Banani et al., 2017), we purified the LCD of RBGD2 (residues 182–404 aa) and RBGD4 (residues 188–411 aa) and examined their capability of LLPS. Like FL RBGD2/4, the LCD from RBGD2/4 could form spherical droplets *in vitro* (Figure 3G). Thus, these data demonstrate that the LCD of RBGD2/4 is sufficient to drive LLPS.

Next, we sought to pinpoint the key residues for LLPS within the LCD of RBGD2 and RBGD4. We used the PLAAC algorithm to identify all the LCD sequences in the *Arabidopsis* proteome (Lancaster et al., 2014). Amino acid composition analyses of LCD indicated that LCDs from RBGDs contained higher portions of glycine (Gly) and tyrosine (Tyr) residues compared with the proteome level (Figure S4A). Notably, Tyr is nearly evenly distributed from the N to C terminus of the LCD of both RBGD2/4 (Figures 4A and S4B), which we term “Tyr residue array (TRA).” The TRA of RBGD2-LCD consists of 22 Tyr residues (9.91% of the LCD), and TRA of RBGD4-LCD contains 25 Tyr residues (11.21% of the LCD). In human RBPs, Tyr is well characterized by a potent capability for driving protein LLPS through hydrophobic interactions (e.g., π - π interaction) of its aromatic side chain (Murthy et al., 2019; Wang et al., 2018a; Krainer et al., 2021). Moreover, Tyr-mediated hydrophobic interactions have been shown to be regulated by temperature (Dignon et al., 2019). Thus, we suspected that Tyr residues in LCDs of RBGD2/4 can supply adequate intermolecular interactions to drive LLPS and also contribute to temperature-dependent LLPS.

We mutated half or all of the Tyr residues (11 or 22 of 22) to Ala in RBGD2-LCD as well as nearly half or all of the Tyr residues (12 or 25 of 25) in RBGD4-LCD (Figures 4A, 4B, and S4C). Strikingly, these TRA mutants could severely impair or even completely

abolish RBGD2/4 LLPS ability both under heat condition and in 15% dextran 70 (Figures 4B, 4C, S4D–S4F). To further explore whether specific Tyr residues within the LCD are responsible for LLPS, we generated 4 variants of RBGD2 or RBGD4. Each of them contains a deletion that results in a loss of 4–6 Tyr residues within the LCD (named D1–D4; Figure S4B). We prepared these variant proteins to high purity *in vitro*. Notably, all the D1–D4 variants of RBGD2 and RBGD4 exhibit modestly reduced capacities of LLPS compared with their TRA mutants *in vitro* (Figures S4D–S4F). Together, these results demonstrate that both RBGD2 and RBGD4 utilize the TRA rather than specific Tyr residues within LCD to drive their LLPS.

TRA in LCD is responsible for mediating RBGD2/4 LLPS *in vivo*

Since we found that TRA in LCDs drives RBGDs LLPS *in vitro*, we next sought to test whether TRA is necessary for the LLPS of RBGD2/4 in plant cells. We generated native promoter-driven 11Ym and 22Ym versions of RBGD2 in plants. We found that RBGD2-11Ym-YFP formed less granules, whereas RBGD2-22Ym-YFP lost the ability to form observable granules after heat treatment (Figures 4D and 4E), despite the fact that their transcripts are expressed at similar levels as the endogenous RBGD2 (Figure 4F). We also produced RBGD2 and RBGD4 overexpression lines harboring the TRA mutations. We confirmed that the TRA mutant proteins are expressed at levels comparable with the WT protein (Figure 4G), with their transcript levels roughly 10-fold and 35-fold higher than the endogenous *RBGD2* and *RBGD4* (Figure S5A). Similar to the results observed for RBGD2 TRA mutants expressed at endogenous levels, Tyr to Ala mutations of RBGD2/4 significantly impaired their abilities to form granules in response to HS (Figures 4H and S5B). Quantification of the number of RBGD-containing granules per cell showed that RBGD2-11Ym retained significantly lower numbers of granules compared with WT ($p < 0.01$) (Figure 4I), whereas no heat-induced granules were detected in RBGD2-22Ym, RBGD4-12Ym, or -25Ym plants (Figures 4H, 4I, and S5B). Of note, replacement of multiple Tyr by Ala in RBGD2/4 did not influence their protein level in cells before or after heat treatment (Figure S5C).

To further examine how mutation of TRA disrupts heat-induced LLPS of RBGD2/4, we constructed both WT and TRA mutants of RBGD2/4 proteins with distinct tags and performed a coimmunoprecipitation (coIP) experiment to detect the homotypical interaction of them under normal and heat conditions

(B and C) Representative DIC images (B) and turbidity measurement (C) show that TRA mutants affect LLPS of RBGD2/4 under 20- μ M proteins, 100-mM NaCl, pH 7.5 at 44°C *in vitro*. Scale bars, 5 μ m. Data are presented as mean \pm SEM, $n = 3$.

(D) Fluorescent images showing subcellular localization of native promoter-driven TRA mutants of *RBGD2-YFP* before and after 30-min heat treatment. Scale bars, 10 and 2 μ m (zoom in).

(E) Quantification of the number of RBGD granules per cell under HS in (D). Data are presented as mean \pm SD, *pRBGD::RBGD2-YFP/rbgd2-1* (WT [$n = 30$], 11Ym [$n = 30$], 22Ym [$n = 30$]), ND, not detected.

(F) Quantified transcript levels of *RBGD2* in WT and transgenic plants in (D). Transcript quantity is relative to *ACT2*; error bars represent the \pm SD of triplicate reactions.

(G) Immunoblots showing the level of WT- and Tyr-mutated RBGD2/4 proteins in overexpression lines. Actin was used as a loading control.

(H) Subcellular localization of overexpressed *RBGD2/4* WT or TRA mutants under control and HS conditions. Scale bars, 2 μ m.

(I) Quantification of the number of RBGD granules per cell under HS in (H). Data are presented as mean \pm SD, *RBGD2-GFP* (WT [$n = 46$], 11Ym [$n = 48$], 22Ym [$n = 10$]), *RBGD4-GFP* (WT [$n = 10$], 12Ym [$n = 15$], 25Ym [$n = 15$]). ND, not detected.

(J and K) CoIP and western blot analyses showing the effects of TRA mutations on homotypical interactions among RBGD2 proteins (J) and RBGD4 proteins (K) under control and HS conditions in *Arabidopsis* protoplasts.

Statistically significant differences with respect to WT are indicated by the double asterisk ($p < 0.01$). See also Figures S4 and S5.

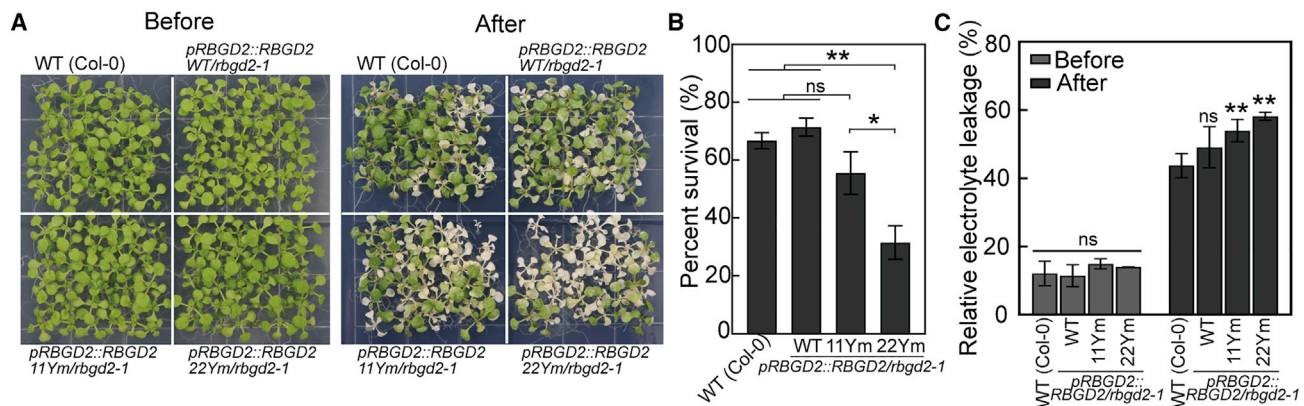


Figure 5. LLPS of RBGD2/4 is essential for their function in heat resistance

(A) Images of WT and transgenic *RBGD2* (WT, 11Ym, and 22Ym) plants before and after heat treatment using the condition in Figure 1B. (B) Calculated survival rates of WT or *pRBGD2::RBGD2* (WT, 11Ym and 22Ym) plants after heat treatment. Data are presented as mean \pm SD. $n = 3$. (C) Relative electrolyte leakage of *RBGD2* WT and TRA mutant complementation lines. Data are presented as mean \pm SD. $n = 3$. Statistically significant differences with respect to the control (WT [Col-0]) are indicated as: * $p < 0.05$ and ** $p < 0.01$. See also Figure S5.

in *Arabidopsis* protoplasts. The results showed that HS promoted the protein homotypical interaction between GFP- and 3xFLAG-tagged RBGD2 WT (Figure 4J). In contrast, this homotypical interaction was almost abolished between GFP- and 3xFLAG-tagged RBGD2-22Ym at the same condition (Figure 4J). Similar results were observed for RBGD4 WT and RBGD4-25Ym proteins (Figure 4K). Together, these *in planta* data demonstrate that TRA in the LCD mediates heat-triggered homotypical interaction of RBGD2/4, which is the main determinant for RBGD2/4 LLPS under HS.

LLPS of RBGD2/4 is essential for their function in HS

We next examined whether LLPS of RBGD2/4 is responsible for their function in protecting plants from HS. We examined the effect of RBGD2 TRA mutants on plant heat resistance. While expression of WT RBGD2 in the *rbgd2-1* mutant restored the survival rate to WT levels, *RBGD2-11Ym* and *RBGD2-22Ym* plants exhibited significantly impaired protective ability against HS (Figure 5A). The *RBGD2-22Ym* plants showed even lower survival rate after HS than that of *RBGD2-11Ym* ($p < 0.05$) (Figure 5B). Consistently, both TRA mutants had higher levels of electrolyte leakage compared with the WT (Figure 5C). As the LLPS capacity of RBGD2 proteins decreased in 11Ym and 22Ym compared with WT (Figure 4), the corresponding transgenic plants showed decreased survival rates and increased electrolyte leakage after HS (Figures 5B and 5C). Thus, the protective effects of RBGD2s were positively correlated with their LLPS capabilities. Meanwhile, overexpression of LLPS-deficient TRA mutants, including *RBGD2-11Ym*, *RBGD2-22Ym*, *RBGD4-12Ym*, and *RBGD4-25Ym*, failed to significantly enhance heat resistance in the WT background (Figures S1F and S5D–S5G). These results indicated that LLPS of RBGD2/4 is necessary for their functions in plant heat resistance.

Characterization of the protein interactome of RBGD2/4

To further dissect the mechanism by which RBGD2/4 promote heat resistance, we attempted to identify the components of RBGD2/4-containing granules. We performed affinity purifica-

tion coupled with mass spectrometry (AP-MS) to identify the proteins that interact with RBGD2-GFP and RBGD4-GFP before and after heat treatment. Consistent with the observation that the majority of RBGD2 and RBGD4 are colocalized in the cell (Figure S2F), proteins that are respectively associated with RBGD2 and RBGD4 are highly similar (Figures S6A and S6B). We thus considered proteins that interact with both RBGD2 and RBGD4 for further analyses. We found 37 proteins under normal temperature and 91 proteins during heat treatment that copurified with both RBGD2 and RBGD4 (Figures S6A and S6B; Table S1). Intriguingly, basically, all the RBGD2/4-associated proteins under room temperature (36 of 37) remain associated with RBGD2/4 during heat treatment (Figure 6A). Albeit 55 more proteins were identified during HS, the RBGD2/4-associated proteins belong to the same functional groups before and after HS, including RBPs, ribosomal proteins, TIFs, HSPs, RNA-processing factors, and proteins involved in basic metabolism (Figure 6B; Table S1). Examination of the STRING database (<https://string-db.org>) identified an extensive PPI network within and among different functional groups (Figure 6B). Many of these proteins are known SG components in plants. Classical SG marker proteins including poly(A) binding protein 2 (PAB2), PAB4, and PAB8 remain associated with RBGD2/4 under both normal and HS conditions; other SG components such as TSN1, TSN2, and EIF2 GAMMA only interact with RBGD2/4 after HS (Figure 6B). Similar functional groups of proteins were also identified as RNA granule components in proteomics-based studies in human (Khong et al., 2017; Markmiller et al., 2018).

In order to verify the AP-MS results, we first examined the localization of RBGD2 (fused to GFP) with PAB8 (fused to RFP) before and after heat treatment in *Arabidopsis* protoplasts. Fluorescent signals of RBGD2 and PAB8 strongly overlapped under both conditions and changed from a dispersed pattern into SGs upon heat treatment (Figure 6C). Using the same method, we also verified the colocalization of TSN1 and TSN2 with RBGD2 under HS (Figures S6C and S6D). In contrast, most signals of RBGD2 did not overlap with DCP1, which is a protein marker of processing bodies (PBs) and was not identified in the

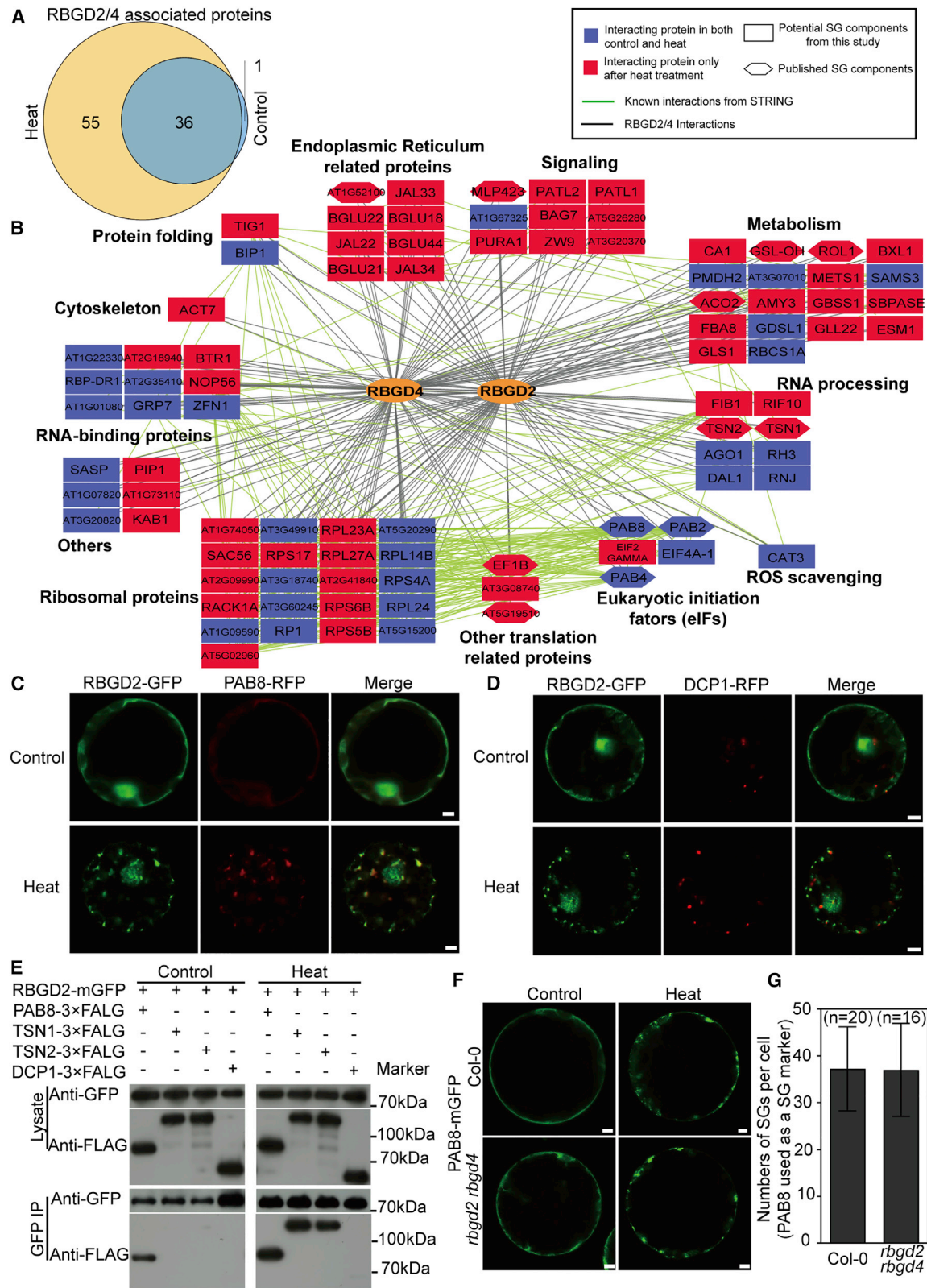


Figure 6. Identification of RBGD2/4 associated proteins before and after heat treatment
(A) Venn diagram showing the number of RBGD2/4-associated proteins before and after heat treatment.
(B) RBGD2/4-associated PPI networks before and after heat treatment.

(legend continued on next page)

RBGD2/4 interactome under either normal or HS conditions (Figure 6D; Table S1). The same colocalization patterns were also observed for RBGD4 under HS (Figures S6E–S6H). These results indicate that RBGD2/4-containing granules are bona fide SGs. We also performed Co-IP experiments to verify the interactions between RBGD2/4 and those marker proteins. Cotransfection of RBGD2-mGFP or RBGD4-mGFP together with FLAG-tagged PAB8, TSN1, TSN2, and DCP1 in *Arabidopsis* protoplasts followed by Co-IP identifies that RBGD2/4 interact with PAB8 under both control and HS conditions (Figures 6E and S6I); interactions between RBGD2/4 and TSN1 or TSN2 were only detected under heat but not control conditions (Figures 6E and S6I), and RBGD2/4 did not interact with DCP1 under control or HS conditions (Figures 6E and S6I). These results were consistent with the protein interactome and colocalization assays. Together, our data demonstrate that RBGD2/4 may cophasse separate with a variety of SG-containing proteins and condense into SGs for heat resistance.

We further tested if RBGD2 and RBGD4 were required for SG formation in plants. The SG marker PAB8 was used to quantify the number of SGs under HS in both WT and *rbgd2 rbgd4* protoplasts. As shown in Figure 6F, HS induced the formation of SGs in both WT and *rbgd2 rbgd4* protoplasts. Quantification of the number of SGs per cell identified no difference between WT and *rbgd2 rbgd4* protoplasts (Figure 6G). Together, our results indicate that RBGD2/4 do not serve as scaffold proteins for plant SG formation.

RBGD2/4 mediate the interaction network with heat-responsive transcripts under HS

Both RBGD2 and RBGD4 are typical RBPs containing two RRM, and the SGs are known to recruit translation-stalled RNP (ribonucleoprotein) complexes. We thus sought to determine the transcripts associated with RBGD2/4 using RIP-seq (RNA immunoprecipitation sequencing). Using RNA-seq data from the input as a covariant, we identified very similar sets of transcripts associated with RBGD2 and RBGD4, suggesting that their RRM domains have similar RNA binding specificity (Figures S7A–S7D). We identified 217 and 250 transcripts that were associated with RBGD2/4 before and after HS, respectively (Figure 7A; Table S2). Around 68% (148/217) of the RBGD2/4-associated transcripts at normal temperature remain associated with RBGD2/4 at the high temperature (Figure 7A). Gene ontology (GO) analyses of the common transcripts at normal and HS conditions identified genes involved in basic plant metabolism such as photosynthesis (Figure 7B; Table S3). HS-specific RBGD2/4-associated transcripts are enriched in genes involved in HS and oxidative stress response, which is consistent with the role of RBGD2/4 in promoting heat resistance (Figure 7C; Table S3). These transcripts include master transcription

factors such as *HSFA2*, *HSF4*, and *HSFA7A*; HSPs such as *HSP18.2*, *HSP81.2*, and *HSP70-HSP90* organizing protein (HOP) *HOP3*; copper homeostasis proteins such as *copper chaperone (CCH)*; and oxidative stress-defending proteins such as *glutathione S-transferase U5 (GSTU5)* and *glutathione S-transferase U19 (GSTU19)* (Figure 7D). Only specific HS-induced transcripts were identified in the RIP-seq results; for example, *HSFA1D/E* transcripts were not enriched after the immunoprecipitation (Figure 7D), indicating high selectivity of the binding of RBGD2/4 to transcripts. Those transcripts exhibit very similar levels in WT or *rbgd2 rbgd4* plants under both control and HS conditions (Figure S7E). Together, by combining the proteomics and RIP-seq results, our work implies that heat-induced LLPS of RBGD2/4 facilitates the assembly of heat-responsive SG components and heat-induced transcripts into SGs to promote HS response.

DISCUSSION

Previous studies showed that protein LLPS contributed to cellular stress resistance in yeast (Maharana et al., 2018; Riback et al., 2017). Whether protein LLPS can serve as a stress-resistant strategy in multicellular organisms is worthy of investigation. In this study, we found that RBGD2 and RBGD4 function redundantly to promote HS resistance in *Arabidopsis* and their ability of LLPS is necessary for this function. Moreover, we provide evidence that the number of, but not that a few specific positioned Tyr residues in the LCD, is critical for the LLPS of RBGD2/4 proteins *in vitro*. Mutations of these Tyr residues (TRA) to Ala disrupt heat-induced formation of RBGD2/4 granules as well as homotypical interaction among RBGD2 and RBGD4 proteins. Identification of TRAs as the key driver for protein LLPS enables us to directly assess the cause-effect relationship between RBGD2/4 LLPS and their activities in HS resistance. Indeed, disruption of the LLPS capacity of RBGD2/4 damages their condensation in heat-induced SGs and directly impairs their ability to promote heat resistance in *Arabidopsis*, strengthening the important role of RBGD2/4 LLPS in HS resistance in plants (Figure S7F).

RBGD2/4 exhibit capacities for phase separation both *in vitro* and *in vivo* under HS (Figures 2A, 2C, and 3B). Enhancement of Tyr-mediated hydrophobic interaction with temperature increase may contribute to RBGD2/4 heat-induced phase separation (Dignon et al., 2019). FRAP experiments showed that RBGD2/4 form dynamic condensates instead of inert protein aggregates. However, heat-induced RBGD2/4-containing granules in the plant cell, but not the heat-induced droplets containing purified RBGD2/4 proteins formed *in vitro*, feature rapid dissociation as temperature decreases. We suspect that other factors such as chaperones are needed to facilitate the

(C) Subcellular colocalization of RBGD2 with the SG marker PAB8 in *Arabidopsis* protoplasts before and after heat treatment. Of note, PAB8 is distributed in cytosol under normal condition, but there are a small portion of PAB8 that is redistributed to nucleus with overexpressed RBGD2. Scale bars, 5 μ m.

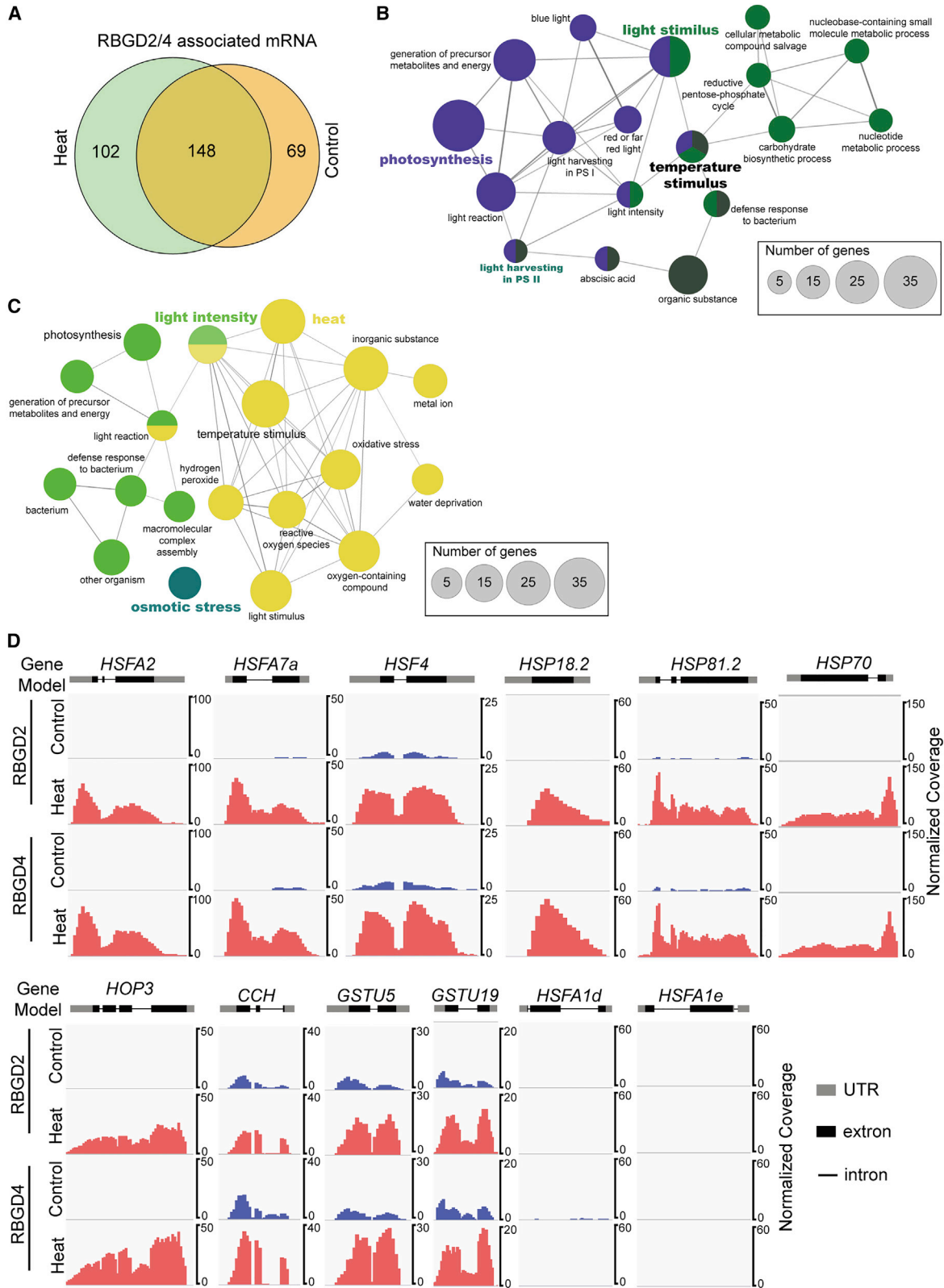
(D) Subcellular colocalization of RBGD2 with the PB marker DCP1 in *Arabidopsis* protoplast before and after heat treatment. Scale bars, 5 μ m.

(E) Co-IP showing the interaction between RBGD2 and marker proteins (PAB8, TSN1, TSN2, and DCP1) under control and HS conditions in *Arabidopsis* protoplasts.

(F) Formation of heat induced SGs in WT and *rbgd2 rbgd4* protoplasts. PAB8 is a marker for SGs. Scale bars, 5 μ m.

(G) Quantification of heat-induced SGs in WT and *rbgd2 rbgd4* protoplasts. Data are presented as mean \pm SD.

See also Figure S6 and Table S1.



(legend on next page)

disassembly of RBGD granules *in vivo*, as have been reported in mammalian cells (Gwon et al., 2021; Li and Liu, 2022). A number of RBGD2/4-associated proteins (e.g., TSN1/2) also form heat-induced SGs *in vivo* (Gutierrez-Beltran et al., 2015) (Table S1), which may act together to facilitate condensation, dynamic-phase maintenance, and function of RBGD2/4 against HS. Importantly, despite the fact that condensation of RBGD2/4 into SGs is important for heat resistance, RBGD2/4 are not required for SG formation in plant cells (Figures 6F and 6G). Whether the composition and/or assembly dynamics of heat-induced SGs are affected by the loss of RBGD2 and RBGD4 is an important question to be explored in the future. RBGD2/4 can also undergo LLPS *in vitro* under cold condition (Figure S3A). However, we did not observe evident granule-like structures formed by either RBGD2 or RBGD4 proteins under cold treatment in cells (Figure S2E). Compared with HS, cold treatment may induce a different cellular environment in plant cells, which we suspect in turn modulates LLPS behavior of RBGD2/4 in different ways.

Compared with the list of SG components recently identified in yeast and mammalian cells (Khong et al., 2017; Markmiller et al., 2018), less is known about the molecular composition of SGs in plants. Here, we demonstrate that RBGD2/4 are components of heat-induced SGs in plants. RBGD2/4 are associated with classical SG marker proteins, but not PB marker proteins such as DCP1 (Figures 6 and S6). AP-MS analyses identified extensive association of RBGD2/4 with well-known plant SG markers including PAB2, PAB4, PAB8, and eIF4A1 under normal conditions (Bogamuwa and Jang, 2013; Koguchi et al., 2017; Kosmacz et al., 2019; Lokdarshi et al., 2016; Merret et al., 2017; Pomeranz et al., 2010; Sorenson and Bailey-Serres, 2014). This pre-existing PPI network among SG components is consistent with recent large-scale proteomics studies in mammalian SGs and may play an important role in accelerating the formation of functional SGs in response to stress (Markmiller et al., 2018). After HS, granule formation significantly increases the number of RBGD2/4-interacting proteins (Figures 6A and 6B). The HS-induced RBGD2/4-associated proteins include additional SG proteins such as TSN1 and TSN2 (Gutierrez-Beltran et al., 2015), confirming that RBGD2/4-containing granules represent typical heat-induced SGs. Our list also contains homologs to some well-known SG proteins in mammals (Chantarachot and Bailey-Serres, 2018). One such protein is AGO1, which is the main Argonaute protein responsible for microRNA processing in plants and was recently shown to coreside with the SG marker PAB8 upon heat treatment (Wang et al., 2018b). Further studies on how these proteins interplay with RBGD2/4 will provide mechanistic insights in the formation and function of plant SGs. Interestingly, RBGD2/4 were not identified in the interactome of Rbp47b, a core component of SGs under HS (Kosmacz et al., 2019). We compared the RBGD2/4-interacting proteins

with the Rbp47b interactome and found that 12 of 91 (13%) RBGD2/4-associated proteins were also identified in Rbp47b interactome, which contained well-known SG markers in plants, such as PAB2/4/8, eIF4A, and TSN1/2 (Figure 6B; Table S2). The differences between RBGD2/4 and Rbp47b interactomes may lie in the distinct biophysical properties of these proteins and their different roles in the complex/dynamic structures of SGs.

We also characterized RBGD2/4-associated mRNAs under both normal and HS conditions. RBGD2/4 bound transcripts are mostly involved in primary metabolism under normal conditions (Figure S7B). After heat treatment, a number of heat-responsive mRNAs become associated with RBGD2/4 (Figures 7C and 7D). Considering that the core structure of SGs is quite stable and the observation that RBGD2/4 interact with a number of RBPs under both normal and HS conditions, current data could not distinguish RNAs directly bound by RBGD2/4 from the ones associated with RBGD2/4 indirectly. However, these results suggest a mechanism by which LCD-mediated LLPS promotes the assembly of heat-responsive and RBGD2/4-bound mRNAs into SGs (Figure S7F). Although the fate of these transcripts in the SGs remains to be determined, SGs seem to promote their function because disrupting the LLPS ability of RBGD2/4 also abolished their effects of promoting heat resistance.

Similar to RBGD2/4, the other three members of the RBGD family (RBGD1, RBGD3, and RBGD5) are also composed of two RRM domains and a disordered LCD (Peng et al., 2006), suggesting that LLPS is a common feature shared by all members (Figures S3E and S3F). However, unlike RBGD2/4, RBGD1, RBGD3, and RBGD5 contain the typical nuclear localization sequences, indicating that they may mainly localize in the nucleus (Figure S3F). Intriguingly, Cao and co-workers found that RBGD5 (also called HLP1) is involved in the regulation of plant flowering time by regulating alternative polyadenylation (Zhang et al., 2015). A recent study also shows that FCA forms nuclear bodies and is essential for alternative polyadenylation (Fang et al., 2019). Thus, it is possible that RBGD5 and FCA participate in the same nuclear body to regulate 3' processing of specific transcripts. Further studies on how different RBGD subgroups participate in different MLO function and the mechanisms by which MLOs function in various biological processes will be of importance.

Limitations of the study

In this study, we found that the TRAs of RBGD2 and RBGD4 are required for phase separation *in vitro* and heat-induced formation of RBGD2/4-containing granules *in vivo*. Whether TRAs is specific for recruitment of RBGD2/4 to SGs but not other MLOs, such as PBs, is not investigated by the current experimental design.

Figure 7. RBGD2/4 bind to specific transcripts before and after heat treatment

- (A) Venn diagram showing the number of RBGD2/4-bound transcripts before and after heat treatment.
(B and C) Enriched GO terms of RBGD2/4-bound transcripts that are associated with RBGD2/4 under both control and HS conditions (B) and only under the HS condition (C). GO terms with very similar (50% similar genes for group merge; 50% similar terms for group merge) set of genes are indicated by the same color and related (κ score ≥ 0.25) GO terms are connected by lines.
(D) IGV genome browser snapshots of normalized coverage of heat-responsive transcripts after RBGD2/4 RIP-seq.
See also Figure S7 and Tables S2 and S3.

STAR★METHODS

Detailed methods are provided in the online version of this paper and include the following:

- **KEY RESOURCES TABLE**
- **RESOURCE AVAILABILITY**
 - Lead contact
 - Materials availability
 - Data and code availability
- **EXPERIMENTAL MODEL AND SUBJECT DETAILS**
 - Plant materials and growth conditions
- **METHOD DETAILS**
 - RNA extraction and qRT-PCR
 - Vector construction
 - Polygenetic tree analyses
 - Recombinant protein expression and purification
 - *In vitro* LLPS assay
 - Turbidity measurement
 - Fluorescent labeling of purified proteins
 - Heat stress treatment
 - Relative electrolyte leakage assay
 - Fluorescent imaging
 - Fluorescence recovery after photobleaching (FRAP) assay
 - Affinity purification coupled mass spectrometry (AP-MS)
 - Co-immunoprecipitation assay
 - RNA-immunoprecipitation (RIP) sequencing and data analyses
- **QUANTIFICATION AND STATISTICAL ANALYSIS**

SUPPLEMENTAL INFORMATION

Supplemental information can be found online at <https://doi.org/10.1016/j.devcel.2022.02.005>.

ACKNOWLEDGMENTS

This work was supported by the National Natural Science Foundation of China (NSFC) (grant no. 82188101 to C.L.), the Major State Basic Research Development Program (grant no. 2019YFE0120600 to C.L.), the Strategic Priority Research Program of CAS (grant no. XDB27040108 to H.Z.), the Belt and Road Program of CAS (grant no. 131965KYSB20190083-03 to H.Z.), the Science and Technology Commission of Shanghai Municipality (STCSM) (grant nos. 18JC1420500, 20XD1425000, and 2019SHZDZX02 to C.L.), the Youth Innovation Promotion Association CAS (grant no. Y201844 to H.Z.), the Excellent Young Scientist Fund of NSFC (grant no. 31922008 to H.Z.), the “Eastern Scholar” project supported by the Shanghai Municipal Education Commission to D.L., the National Natural Science Foundation of China (grant nos. 91853113 and 31872716 to D.L. and C.L. and 32170683 to D.L.), Shanghai Pilot Program for Basic Research—Chinese Academy of Science, Shanghai Branch (grant no. JCYJ-SHFY-2022-005 to C.L.), the Joint Funds of the National Natural Science Foundation of China (grant no. U1932204 to C.L.), and the CAS project for Young Scientists in Basic Research (grant no. YSBR-009).

AUTHOR CONTRIBUTIONS

C.L. and H.Z. designed the project. S.Z., Z.W., Z.Z., J.Y., and L.L., performed all *in vivo* plant-related experiments. J.G., Y.L., X.G., W.X., and D.L. performed the *in vitro* biochemical characterization of protein LLPS. All the authors were

involved in analyzing the data and contributed to manuscript discussion and editing. C.L. and H.Z. wrote the manuscript.

DECLARATION OF INTERESTS

The authors declare no competing interests.

Received: December 2, 2020

Revised: August 24, 2021

Accepted: February 2, 2022

Published: February 28, 2022

REFERENCES

- Ambrosone, A., Costa, A., Leone, A., and Grillo, S. (2012). Beyond transcription: RNA-binding proteins as emerging regulators of plant response to environmental constraints. *Plant Sci.* 182, 12–18.
- Banani, S.F., Lee, H.O., Hyman, A.A., and Rosen, M.K. (2017). Biomolecular condensates: organizers of cellular biochemistry. *Nat. Rev. Mol. Cell Biol.* 18, 285–298.
- Battisti, D.S., and Naylor, R.L. (2009). Historical warnings of future food insecurity with unprecedented seasonal heat. *Science* 323, 240–244.
- Bogamuwa, S., and Jang, J.C. (2013). The Arabidopsis tandem CCCH zinc finger proteins AtTZF4, 5 and 6 are involved in light-, abscisic acid- and gibberellic acid-mediated regulation of seed germination. *Plant Cell Environ.* 36, 1507–1519.
- Chakrabortee, S., Kayatekin, C., Newby, G.A., Mendillo, M.L., Lancaster, A., and Lindquist, S. (2016). Luminidependens (LD) is an Arabidopsis protein with prion behavior. *Proc. Natl. Acad. Sci. USA* 113, 6065–6070.
- Chantarachot, T., and Bailey-Serres, J. (2018). Polysomes, stress granules, and processing bodies: a dynamic triumvirate controlling cytoplasmic mRNA fate and function. *Plant Physiol.* 176, 254–269.
- Dignon, G.L., Zheng, W., Kim, Y.C., and Mittal, J. (2019). Temperature-controlled liquid-liquid phase separation of disordered proteins. *ACS Cent. Sci.* 5, 821–830.
- Fang, X., Wang, L., Ishikawa, R., Li, Y., Fiedler, M., Liu, F., Calder, G., Rowan, B., Weigel, D., Li, P., et al. (2019). Arabidopsis FLL2 promotes liquid-liquid phase separation of polyadenylation complexes. *Nature* 569, 265–269.
- Freeman Rosenzweig, E.S., Xu, B., Kuhn Cuellar, L., Martinez-Sanchez, A., Schaffer, M., Strauss, M., Cartwright, H.N., Ronceray, P., Plitzko, J.M., Förster, F., et al. (2017). The eukaryotic CO(2)-concentrating organelle is liquid-like and exhibits dynamic reorganization. *Cell* 171, 148–162.e119.
- Gutierrez-Beltran, E., Moschou, P.N., Smertenko, A.P., and Bozhkov, P.V. (2015). Tudor staphylococcal nuclease links formation of stress granules and processing bodies with mRNA catabolism in Arabidopsis. *Plant Cell* 27, 926–943.
- Gwon, Y., Maxwell, B.A., Kolaitis, R.M., Zhang, P., Kim, H.J., and Taylor, J.P. (2021). Ubiquitination of G3BP1 mediates stress granule disassembly in a context-specific manner. *Science* 372, eabf6548.
- Harrison, A.F., and Shorter, J. (2017). RNA-binding proteins with prion-like domains in health and disease. *Biochem. J.* 474, 1417–1438.
- Jain, S., Wheeler, J.R., Walters, R.W., Agrawal, A., Barsic, A., and Parker, R. (2016). ATPase-modulated stress granules contain a diverse proteome and substructure. *Cell* 164, 487–498.
- Khong, A., Matheny, T., Jain, S., Mitchell, S.F., Wheeler, J.R., and Parker, R. (2017). The stress granule transcriptome reveals principles of mRNA accumulation in stress granules. *Mol. Cell* 68, 808–820.e5.
- Koguchi, M., Yamasaki, K., Hirano, T., and Sato, M.H. (2017). Vascular plant one-zinc-finger protein 2 is localized both to the nucleus and stress granules under heat stress in Arabidopsis. *Plant Signal. Behav.* 12, e1295907.
- Kosmacz, M., Gorka, M., Schmidt, S., Luzarowski, M., Moreno, J.C., Szlachetko, J., Leniak, E., Sokolowska, E.M., Sofroni, K., Schnittger, A., et al. (2019). Protein and metabolite composition of Arabidopsis stress granules. *New Phytol* 222, 1420–1433.

- Krainer, G., Welsh, T.J., Joseph, J.A., Espinosa, J.R., Wittmann, S., de Csilléry, E., Sridhar, A., Toprakcioglu, Z., Gudíškýtė, G., Czekalska, M.A., et al. (2021). Reentrant liquid condensate phase of proteins is stabilized by hydrophobic and non-ionic interactions. *Nat. Commun.* **12**, 1085.
- Lancaster, A.K., Nutter-Upham, A., Lindquist, S., and King, O.D. (2014). PLAAC: a web and command-line application to identify proteins with prion-like amino acid composition. *Bioinformatics* **30**, 2501–2502.
- Li, D., and Liu, C. (2022). Spatiotemporal dynamic regulation of membraneless organelles by chaperone networks. *Trends Cell Biol.* **32**, 1–3.
- Lin, Y., Protter, D.S., Rosen, M.K., and Parker, R. (2015). Formation and maturation of phase-separated liquid droplets by RNA-binding proteins. *Mol. Cell* **60**, 208–219.
- Liu, H.C., Liao, H.T., and Charng, Y.Y. (2011). The role of class A1 heat shock factors (HSFA1s) in response to heat and other stresses in *Arabidopsis*. *Plant Cell Environ.* **34**, 738–751.
- Lokdarshi, A., Conner, W.C., McClintock, C., Li, T., and Roberts, D.M. (2016). *Arabidopsis* CML38, a calcium sensor that localizes to ribonucleoprotein complexes under hypoxia stress. *Plant Physiol.* **170**, 1046–1059.
- Maharana, S., Wang, J., Papadopoulos, D.K., Richter, D., Pozniakovskiy, A., Poser, I., Bickle, M., Rizk, S., Guillén-Boixet, J., Franzmann, T.M., et al. (2018). RNA buffers the phase separation behavior of prion-like RNA binding proteins. *Science* **360**, 918–921.
- Markmiller, S., Soltanieh, S., Server, K.L., Mak, R., Jin, W., Fang, M.Y., Luo, E.C., Krach, F., Yang, D., Sen, A., et al. (2018). Context-dependent and disease-specific diversity in protein interactions within stress granules. *Cell* **172**, 590–604.e13.
- Merret, R., Carpentier, M.C., Favory, J.J., Picart, C., Descombin, J., Bousquet-Antonelli, C., Tillard, P., Lejay, L., Deragon, J.M., and Charng, Y.Y. (2017). Heat shock protein HSP101 affects the release of ribosomal protein mRNAs for recovery after heat shock. *Plant Physiol.* **174**, 1216–1225.
- Mishra, S.K., Tripp, J., Winkelhaus, S., Tschiersch, B., Theres, K., Nover, L., and Scharf, K.D. (2002). In the complex family of heat stress transcription factors, HsfA1 has a unique role as master regulator of thermotolerance in tomato. *Genes Dev.* **16**, 1555–1567.
- Molliex, A., Temirov, J., Lee, J., Coughlin, M., Kanagaraj, A.P., Kim, H.J., Mittag, T., and Taylor, J.P. (2015). Phase separation by low complexity domains promotes stress granule assembly and drives pathological fibrillization. *Cell* **163**, 123–133.
- Murthy, A.C., Dignon, G.L., Kan, Y., Zerze, G.H., Parekh, S.H., Mittal, J., and Fawzi, N.L. (2019). Molecular interactions underlying liquid-liquid phase separation of the FUS low-complexity domain. *Nat. Struct. Mol. Biol.* **26**, 637–648.
- Nakaminami, K., Matsui, A., Shinozaki, K., and Seki, M. (2012). RNA regulation in plant abiotic stress responses. *Biochim. Biophys. Acta* **1819**, 149–153.
- Ohama, N., Sato, H., Shinozaki, K., and Yamaguchi-Shinozaki, K. (2017). Transcriptional regulatory network of plant heat stress response. *Trends Plant Sci.* **22**, 53–65.
- Peng, K., Radivojac, P., Vucetic, S., Dunker, A.K., and Obradovic, Z. (2006). Length-dependent prediction of protein intrinsic disorder. *BMC Bioinformatics* **7**, 208.
- Pomeranz, M.C., Hah, C., Lin, P.C., Kang, S.G., Finer, J.J., Blackshear, P.J., and Jang, J.C. (2010). The *Arabidopsis* tandem zinc finger protein AtTZF1 traffics between the nucleus and cytoplasmic foci and binds both DNA and RNA. *Plant Physiol.* **152**, 151–165.
- Protter, D.S.W., and Parker, R. (2016). Principles and properties of stress granules. *Trends Cell Biol.* **26**, 668–679.
- Riback, J.A., Katanski, C.D., Kear-Scott, J.L., Pilipenko, E.V., Rojek, A.E., Sosnick, T.R., and Drummond, D.A. (2017). Stress-triggered phase separation is an adaptive, evolutionarily tuned response. *Cell* **168**, 1028–1040.e19.
- Sorenson, R., and Bailey-Serres, J. (2014). Selective mRNA sequestration by OLIGOURIDYLATE-BINDING PROTEIN 1 contributes to translational control during hypoxia in *Arabidopsis*. *Proc. Natl. Acad. Sci. USA* **111**, 2373–2378.
- Van Treeck, B., Protter, D.S.W., Matheny, T., Khong, A., Link, C.D., and Parker, R. (2018). RNA self-assembly contributes to stress granule formation and defining the stress granule transcriptome. *Proc. Natl. Acad. Sci. USA* **115**, 2734–2739.
- Wang, H., Yan, X., Aigner, H., Bracher, A., Nguyen, N.D., Hee, W.Y., Long, B.M., Price, G.D., Hartl, F.U., and Hayer-Hartl, M. (2019). RuBisCO condensate formation by CcmM in β -carboxysome biogenesis. *Nature* **566**, 131–135.
- Wang, J., Choi, J.M., Holehouse, A.S., Lee, H.O., Zhang, X., Jahnel, M., Maharana, S., Lemaitre, R., Pozniakovskiy, A., Drechsel, D., et al. (2018a). A molecular grammar governing the driving forces for phase separation of prion-like RNA binding proteins. *Cell* **174**, 688–699.e16.
- Wang, X., Wang, Y., Dou, Y., Chen, L., Wang, J., Jiang, N., Guo, C., Yao, Q., Wang, C., Liu, L., et al. (2018b). Degradation of unmethylated miRNA/miRNA*s by a DEDDy-type 3' to 5' exoribonuclease Atrimmer 2 in *Arabidopsis*. *Proc. Natl. Acad. Sci. USA* **115**, E6659–E6667.
- Weber, C., Nover, L., and Fauth, M. (2008). Plant stress granules and mRNA processing bodies are distinct from heat stress granules. *Plant J.* **56**, 517–530.
- Wegmann, S., Eftekharzadeh, B., Tepper, K., Zoltowska, K.M., Bennett, R.E., Dujardin, S., Laskowski, P.R., MacKenzie, D., Kamath, T., Commins, C., et al. (2018). Tau protein liquid-liquid phase separation can initiate tau aggregation. *EMBO J.* **37**, e98049.
- Wolozin, B., and Ivanov, P. (2019). Stress granules and neurodegeneration. *Nat. Rev. Neurosci.* **20**, 649–666.
- Yoshida, T., Ohama, N., Nakajima, J., Kidokoro, S., Mizoi, J., Nakashima, K., Maruyama, K., Kim, J.M., Seki, M., Todaka, D., et al. (2011). *Arabidopsis* HsfA1 transcription factors function as the main positive regulators in heat shock-responsive gene expression. *Mol. Genet. Genomics* **286**, 321–332.
- Zhang, C., Du, X., Tang, K., Yang, Z., Pan, L., Zhu, P., Luo, J., Jiang, Y., Zhang, H., Wan, H., et al. (2018). *Arabidopsis* AGDP1 links H3K9me2 to DNA methylation in heterochromatin. *Nat. Commun.* **9**, 4547.
- Zhang, Y., Gu, L., Hou, Y., Wang, L., Deng, X., Hang, R., Chen, D., Zhang, X., Zhang, Y., Liu, C., et al. (2015). Integrative genome-wide analysis reveals HLP1, a novel RNA-binding protein, regulates plant flowering by targeting alternative polyadenylation. *Cell Res.* **25**, 864–876.
- Zhao, S., Cheng, L., Gao, Y., Zhang, B., Zheng, X., Wang, L., Li, P., Sun, Q., and Li, H. (2019). Plant HP1 protein ADCP1 links multivalent H3K9 methylation readout to heterochromatin formation. *Cell Res.* **29**, 54–66.

STAR★METHODS

KEY RESOURCES TABLE

Reagent or resource	Source	Identifier
Antibodies		
Mouse monoclonal anti-Green Fluorescence Protein antibody	Roche	Cat. No. 11814460001; RRID: AB_390913
Goat Anti-Mouse IgG (H + L)-HRP Conjugate	BioRad	Cat. No. 1706516; RRID: AB_11125547
Monoclonal ANTI-FLAG M2 antibody produced in mouse	Sigma	Cat. No. F1804; RRID: AB_262044
Anti β -Actin Mouse Monoclonal Antibody	CWBIO	Cat. No. F1804
Bacterial and virus strains		
<i>E. coli</i> DH5 α cells	WEIDI	Cat. No. DL1001
<i>Agrobacterium tumefaciens</i> GV3101	WEIDI	Cat. No. AC1001
BL21(DE3) Chemically Competent Cell	TransGen Biotech	Cat. No. CD601-02
Transsetta(DE3) Chemically Competent Cell	TransGen Biotech	Cat. No. CD801-02
Chemicals, peptides, and recombinant proteins		
TRIzol Reagent	Thermo Fisher Scientific	Cat. No. 15596026
EDTA-free, EASYpack Protease Inhibitor Cocktail Tablets	Roche	Cat. No. 04693132001
GFP-Trap_MA	Chromotek	Cat. No. gtma-200
RiboLock RNase Inhibitor	Thermo Scientific	Cat. No. EO0382
Oregon-Green488	Invitrogen	Cat. No. O6149
Alexa Fluor 350 NHS Ester	Invitrogen	Cat. No. A10168
RNase A	Sigma-Aldrich	Cat. No. R4875
DNase I	Ambion	Cat. No. AM2222
Critical commercial assays		
Pierce BCA Protein Assay Kit	Thermo Fisher Scientific	Cat. No. 23225
Deposited data		
Original western blot	Mendeley	https://doi.org/10.17632/t6ctymj5bb.1
RIP-Seq data	NCBI, BioProject	PRJNA799874
Experimental models: Organisms/strains		
<i>Arabidopsis thaliana</i> (Columbia-0)	This paper	N/A
<i>rbgd2-1</i>	Arabidopsis Biological Resource Center (ABRC)	SALK_202494/SALK_040839
<i>rbgd4-1</i>	Arabidopsis Biological Resource Center (ABRC)	WisDsLox461-464K4
<i>rbgd4-2</i>	Arabidopsis Biological Resource Center (ABRC)	WisDsLox413-41619
Oligonucleotides		
See Table S4 for all Primer sequences	This paper	N/A
Recombinant DNA		
His-SUMO-RBGD2-WT	This paper	N/A
His-SUMO-RBGD2-11Ym	This paper	N/A
His-SUMO-RBGD2-22Ym	This paper	N/A
His-SUMO-RBGD2-D1(Δ 222-244 aa)	This paper	N/A
His-SUMO-RBGD2-D2(Δ 245-277 aa)	This paper	N/A
His-SUMO-RBGD2-D3(Δ 327-359 aa)	This paper	N/A
His-SUMO-RBGD2-D4(Δ 366-410 aa)	This paper	N/A

(Continued on next page)

Continued

Reagent or resource	Source	Identifier
His-SUMO-RBGD4-WT	This paper	N/A
His-SUMO-RBGD4-12Ym	This paper	N/A
His-SUMO-RBGD4-25Ym	This paper	N/A
His-SUMO-RBGD4-D1(Δ 208-249 aa)	This paper	N/A
His-SUMO-RBGD4-D2(Δ 253-294 aa)	This paper	N/A
His-SUMO-RBGD4-D3(Δ 306-348 aa)	This paper	N/A
His-SUMO-RBGD4-D4(Δ 354-403 aa)	This paper	N/A
His-RBGD2-LCD	This paper	N/A
Trx1-His-3C-RBGD4-LCD	This paper	N/A
GST-3C	This paper	N/A
His-Ulp1	This paper	N/A
pCambia1300-35S::RBGD2-GFP	This paper	N/A
pCambia1300-35S::RBGD2 11Ym-GFP	This paper	N/A
pCambia1300-35S::RBGD2 22Ym-GFP	This paper	N/A
pCambia1300-35S::RBGD4-GFP	This paper	N/A
pCambia1300-35S::RBGD4 12Ym-GFP	This paper	N/A
pCambia1300-35S::RBGD2 25Ym-GFP	This paper	N/A
pCambia1300-pRBGD2::RBGD2-YFP	This paper	N/A
pCambia1300-pRBGD2::RBGD2 11Ym-YFP	This paper	N/A
pCambia1300-pRBGD2::RBGD2 22Ym-YFP	This paper	N/A
pEZS_NL-RBGD2-GFP	This paper	N/A
pEZS_NL-RBGD4-RFP	This paper	N/A
pEZS_NL-PAB8-RFP	This paper	N/A
pEZS_NL-TSN1-RFP	This paper	N/A
pEZS_NL-TSN2-RFP	This paper	N/A
pEZS_NL-DCP1-RFP	This paper	N/A
pEZS_NL-RBGD2-3xFLAG	This paper	N/A
pEZS_NL-RBGD2 22Ym-3xFLAG	This paper	N/A
pEZS_NL-RBGD4 -3xFLAG	This paper	N/A
pEZS_NL-RBGD4 25Ym-3xFLAG	This paper	N/A
pEZS_NL-PAB8-3xFLAG	This paper	N/A
pEZS_NL-TSN1-3xFLAG	This paper	N/A
pEZS_NL-TSN2-3xFLAG	This paper	N/A
pEZS_NL-DCP1-3xFLAG	This paper	N/A

Software and algorithms

GraphPad Prism	GraphPad Software Inc Prism	https://www.graphpad.com/scientific-software/prism/ , RRID: SCR_002798
----------------	-----------------------------	--

RESOURCE AVAILABILITY

Lead contact

Further information and requests for resources should be directed to and will be fulfilled by the lead contact Cong Liu (liulab@sioc.ac.cn).

Materials availability

All unique reagents generated in this study will be available from the lead contact.

Data and code availability

- RIP-Seq data have been deposited at NCBI BioProject and are publicly available as of the date of publication. The accession number is listed in the [key resources table](#). Original western blot images have been deposited at Mendeley and are publicly available as of the date of publication. The DOI is listed in the [key resources table](#). The other original data reported in this paper will be shared by the lead contact upon request.

- This paper does not report original code.
- Any additional information required to reanalyze the data reported in this paper is available from the lead contact upon request.

EXPERIMENTAL MODEL AND SUBJECT DETAILS

Plant materials and growth conditions

All the *Arabidopsis thaliana* plants used in this study was in Columbia-0 (Col-0) ecotype. The mutant *rbgd2-1* (SALK_202494/SALK_040839), *rbgd4-1* (WisDsLox461-464K4) and *rbgd4-2* (WiscDsLox413-41619) were obtained from *Arabidopsis Biological Resource Center* (ABRC). For seedlings grown on plates, seeds were sown on 1/2 Murashige and Skoog (MS) medium plates (1% sucrose, 0.7% agar), kept at 4°C in the darkness for 2 days before being moved to the growth chamber (Percival, CU-36L5) with long-day growth conditions (16 h - 8 h / 22°C - 20°C, day-night cycle).

METHOD DETAILS

RNA extraction and qRT-PCR

RNA extraction, cDNA synthesis and real-time PCR were performed using kits following the manufacturers' standard procedures. Specifically, total RNA was extracted from seedling or specific organs using RNeasy Plant Mini Kit (Qiagen, Cat. No. 74904). The cDNA was reverse transcribed from 2-μg total RNA with oligo(dT) primers using TransScript One-Step gDNA Removal and cDNA Synthesis SuperMix kit (TransGen, Cat. No. AT311-03). The real-time-PCR was performed with ChamQ Universal SYBR qPCR Master Mix (Vazyme, Cat. No. Q711-02) on a Quick Plate_96 wells_SYBR Only system (BioRad). For data analyses, we used the delta CT (critical threshold) method and the mRNA level of *ACT2* (AT5G09810) was used as an internal reference. The primer sequences used are listed in [Table S4](#).

Vector construction

The coding sequences (CDS) of *RBGD2* (AT2G33410) and *RBGD4* (AT4G14330) were amplified by PCR from Col-0 cDNA (primers shown in [Table S4](#)). The artificial CDS of *RBGD2-11Ym*, *RBGD2-22Ym*, *RBGD4-12Ym* and *RBGD4-25Ym* were synthesized at Gen-eray (Shanghai, China) and designed to mutate specific tyrosines (Y) to alanines (A) as indicated in [Figure S4](#). All the CDS sequences without the stop codon, together with an upstream cauliflower mosaic virus 35S promoter sequence and an downstream GFP CDS sequence, were cloned into the pCambia1300 vector through homologous recombination using ClonExpress Ultra One Step Cloning Kit (Vazyme, Cat. No. C115-01). To generate *pRBGD2::RBGD2-YFP* transgenic lines in the *rbgd2* mutant, genomic sequence from upstream 1689 bp to the nucleotide before the start codon of *RBGD2*, the CDS sequence of YFP, and 1000 bp sequence after the stop codon of *RBGD2* were homologously recombined into the pCambia1300 vector, which was linearised using *EcoRI* and *Sall* restriction endonucleases. The tyrosines mutants *pRBGD2::RBGD2-11Ym-YFP* and *pRBGD2::RBGD2-22Ym-YFP* were constructed in a similar way. All the vectors described above were transformed into *Agrobacterium tumefaciens* strain GV3101 (WEIDI, Cat. No. AC1001) for genetic transformation of *Arabidopsis* plants using the floral-dip method.

For the analysis on subcellular localization of RBGD proteins, the CDS of *RBGD2*, *RBGD4*, *PAB8* (AT1G49760), *TSN1* (AT5G07350), *TSN2* (AT5G61780) and *DCP1* (AT1G08370) were cloned and homologously recombined into pEzS_NL, which was linearised using *EcoRI* and *KpnI* restriction endonucleases. Protoplasts were isolated from the leaves of four-week-old *Arabidopsis* plants. The *35S::RBGD2-GFP* and *35S::RBGD4-RFP*, *35S::PAB8-RFP*, *35S::TSN1-RFP*, *35S::TSN2-RFP* or *35S::DCP1-RFP* constructs in the pEzS_NL backbone were co-transformed into the protoplasts and incubated at 22°C in the dark for 12 - 18 h. Fluorescent signals from the protoplasts were then examined under a fluorescent confocal microscope (Leica TSC SP8) at the Facility for Cell Biology at Shanghai Center for Plant Stress Biology.

Polygenetic tree analyses

The phylogenetic tree was generated using alignments of the RRM domain sequences in MEGA with a neighbor-joining method. Numbers at branching points indicate bootstrap values determined from 1000 repetitions.

Recombinant protein expression and purification

For recombinant protein expression in *E. coli*, full-length *RBGD2/4* CDS and the TRA mutations were clone into the pET28a vector with an N-terminal His-SUMO tag. The vectors for *RBGD2/4* deletion mutants, including *RBGD2 D1-D4*, *RBGD4 D1-D4* were generated from *RBGD2/4* WT vectors. *RBGD2-LCD* (corresponding to residues 182-404 aa) was cloned into the pET28a vector with an N-terminal His tag. And *RBGD4-LCD* (corresponding to residues 188-414 aa) was cloned into pET32a vector with an HRV 3C protease cleavable N-terminal Trx1-His tag.

Full-length *RBGD2/4* and their mutants were expressed at 25°C for 13 h with 0.5 mM IPTG induction. Cells were harvested and lysed in 50 mM Tris-HCl (pH 7.5), 500 mM NaCl, 12.5 mM imidazole, 2 mM PMSF and 0.1 mg/ml RNase A. After removing the cell pellet, supernatant was loaded onto a Ni column (GE Healthcare, USA). The bound protein was next eluted in an elution buffer (50 mM Tris-HCl, 500 mM NaCl, pH 7.5, and 500 mM imidazole). The His-SUMO tag was cleaved off using the His-Ulp1 protease during dialysis against the dialysis buffer (50 mM Tris-HCl, 500 mM NaCl, pH 7.5 and 5 % glycerol) at room temperature for 4 h.

Then proteins were injected to a Ni column to remove the cleaved His-SUMO tag and uncleavage protein. Finally, purified proteins were concentrated, aliquoted in PCR tubes, flash-frozen in liquid nitrogen and stored at -80°C .

The LCD of RBGD2/4 were expressed with 1 mM IPTG at 37°C for 18 h. Cells were lysed in a buffer containing 50 mM Tris-HCl, pH 7.5 and 100 mM NaCl. The pellet after centrifugation (16000 rpm, 4°C , 1 h) was dissolved in 50 mM Tris-HCl (pH 8.0), 6 M guanidine hydrochloride with sonication. The resuspended transparent solution was then loaded into a Ni column, and the purified protein was eluted with 50 mM Tris-HCl, pH 8.0, 6 M guanidine hydrochloride and 100 mM imidazole. The eluted protein was further purified by HPLC (Agilent) and freeze-dried in the FreeZone lyophilizer (Thermo Fisher). For RBGD2-LCD, protein powder was dissolved directly in any buffer for downstream analyses. As for Trx1-His-3C-RBGD4-LCD, protein powder was dissolved into reaction buffer containing 50 mM Tris-HCl (pH 7.5) and 100 mM NaCl and Trx1-His tag was cleaved off using the HRV 3C protease with GST tag at room temperature. After centrifugation, the mixture was loaded onto a Ni column and a Glutathione Sepharose column (GE Healthcare, USA) to remove the Trx1-His and protease. Purified proteins in the flow-through were then concentrated and aliquoted.

In vitro LLPS assay

Protein samples of RBGD2/4 and their variants were prepared in LLPS buffers as indicated. Regarding temperature-dependent assays, RBGD2/4 proteins were prepared in a LLPS buffer without crowding effects and incubated in test tubes in a metal bath. The sample was incubated at indicated temperature for at least 5 min before further experiments.

Turbidity measurement

Turbidity of phase separated samples was measured based on the optical absorption at 600 nm. Turbidity measurement of RBGD2/4 proteins under 15% dextran were recorded on a Varioskan Flash spectral scanning multimode reader (Thermo Fisher) using a flat bottom and low volume 384-well plates (Corning). Temperature-dependent phase separation was quantified by a Chirascan CD spectrometer (Applied Photophysics, UK) equipped with temperature-controlled system (Julobo).

Fluorescent labeling of purified proteins

The protein solution was desalted into reaction buffer containing 50 mM sodium phosphate (pH 7.2), 500 mM NaCl and 10% glycerol using a desalting column (GE Healthcare, USA). Proteins were then incubated with 10-fold Oregon-Green488 (Invitrogen, O6149) or Alexa Fluor 350 NHS Ester (Invitrogen, A10168) at room temperature for 1 h. Labeled proteins were further purified using Superdex 75 10/300 columns (GE Healthcare, USA) in a buffer containing 50 mM Tris-HCl, pH 7.5, 500 mM NaCl and 10% glycerol. The unlabeled protein was mixed with the labeled protein with a molar ratio of 49:1 (unlabeled: labeled) for subsequent LLPS assays and confocal imaging.

Heat stress treatment

Twelve-day-old *Arabidopsis* seedlings grown on 1/2 MS plates were treated for 2 days at 38°C with 16 h-8 h day-night cycle or 4.5-hrs at 42°C and then allowed to recover for 7 or 10 days at 22°C in the growth chamber (Percival, CU-36L5). At the end of the recovery, photographs were taken and the survival rate was measured. The criterion used to confirm the survival of heat-treated seedlings is to examine the vigor of the shoot apical region after a period (7-10 days) after the heat treatment.

Relative electrolyte leakage assay

Twelve-day-old *Arabidopsis* seedlings grown on 1/2 MS plates were treated for 2 days at 38°C day-night cycle. Then 30 seedlings were immediately transferred into a 50 ml Eppendorf tube and washed three times with ddH₂O. Add 15-ml ddH₂O to each tube, and incubate on a shaker (22°C , 150 rpm) for 2 hours. Then the initial electrolyte leakage (E_i) was measured using Orion StarTM A212 (Thermo Fisher). The electrolyte leakage of ddH₂O (E_{i0}) was used as a background. All the tubes, include ddH₂O, were boiled for 30 min, and the final electrolyte leakage (E_f), include ddH₂O (E_{f0}), were measured after cooling to the room temperature. The relative electrolyte leakage (%) is calculated as $(E_i - E_{i0}) \times 100 / (E_f - E_{f0})$.

Fluorescent imaging

Seven-day-old *Arabidopsis* seedlings were treated at 37°C in a 1.5 ml Eppendorf with 1 ml ddH₂O that was pre-heated on a metal bath for 30 min. For RBGD2/4-GFP granules recovery assay, confocal images were taken every 20 min during recovery from 30-min heat treatment. GFP fluorescence was detected in *Arabidopsis* hypocotyl using Leica TSC SP8 with a 63 \times oil immersion objective or Andor Spinning Disk Revolution WD with 60 \times oil immersion objective (for 3D image). GFP was excited at 488 nm and detected at 500 - 550 nm. RFP was excited at 561 nm and detected at 575 - 625 nm. The fluorescence of GFP and RFP were acquired sequentially to avoid signal contamination.

For LLPS assays, RBGD2/4 and their mutant samples were loaded onto BGSD slides with coverslips and images were acquired on a Leica TCS SP8 microscope with a 100 \times oil immersion objective at room temperature. As for temperature-dependent assay, RBGD2/4 WT were dropped on glass slides placed on a temperature-controlled stage (TP-CHSQ-C Thermal stage) at indicated temperatures.

Fluorescence recovery after photobleaching (FRAP) assay

In plants, the FRAP analysis was performed on a Leica TSC SP8. GFP fluorescence was detected using a 40× oil immersion objective. The FRAP model of Leica TSC SP8 was as follows: for the pre-bleach, one RBGD-containing granule is first recorded with 20 iterations to determine the stability of the signal itself, then the granule was bleached with 5 iterations using a laser intensity of 100% at 405 nm. After bleaching, images were recorded with 50 iterations. The time per-iteration was 1.29 s.

For RBGD2/4 droplets *in vitro*, the FRAP module of the Leica TCS SP8 confocal microscopy was used to acquire FRAP data. In brief, droplets with fluorescent labeled proteins were bleached using the laser beam. After photobleaching, images were continuously captured along time (t) (1 image per 2.58 s). The fluorescent intensity (I_t^m) was recorded on the bleached region. Meanwhile, the fluorescent intensity (I_t^c) of a nearby unbleached droplet was also recorded as a control. At each indicated time point (t), the fluorescence intensity of the bleached region was normalized to the fluorescence intensity of the unbleached region and fluorescence recovery was calculated with the formula: $(I_t^m/I_0^m)/(I_t^c/I_0^c)$.

Affinity purification coupled mass spectrometry (AP-MS)

Affinity purification was performed as described in [Sorenson and Bailey-Serres \(2014\)](#). Briefly, 14-day-old seedlings were treated for 1 h at 37°C in the darkness in the growth chamber (Percival, CU-36L5). The seedlings were harvested and ground into fine powder in liquid nitrogen. The ground powder was then added to ice-cold extraction buffer (200 mM Tris (pH 9.0), 110 mM potassium acetate, 0.5% Triton-X100, 0.1% Tween-20, 1% protease inhibitor cocktail (Roche), 5 mM DTT, 40 u/ml RNase inhibitor (Thermo, Cat. No. E00382)). The tube was briefly vortexed and the protein extract was filtered through two layers of Miracloth (EMD Millipore) into a clean 50-mL tube. The filtrate was centrifuged in a swinging bucket rotor at $\sim 1,500 \times g$ for 2 min at 4°C. The supernatant was transferred to a fresh tube and an aliquot was taken for SDS-PAGE analyses and RNA extraction. Then buffer-balanced GFP-Trap Magnetic Beads (25 μ L) were added to the remaining supernatant. AP of tag-protein-containing complexes was accomplished by rotating the supernatant-beads slurry at 4°C for 1 h. The GFP-Trap beads were then magnetically collected and were washed with 1 mL extraction buffer for 5 min for 5 times at 4°C. After the last wash, a wide-cut pipette tip was used to distribute the bead slurry into three aliquotes: 0.1 mL for SDS-PAGE, 0.45 mL for MS, and 0.45 mL (for RNA extraction).

MS analyses were performed at the Proteomics Facility of Shanghai Center for Plant Stress Biology. For pretreatment of MS samples, 200 μ L GdmCl lysis buffer (6 M GdmHCl (guanidine hydrochloride), 100 mM Tris-HCl (pH = 8.5), 10 mM TCEP, 40 mM CAA (2-chloroacetamide) were added to the beads and boiled at 95°C for 5-10 min in order to denature and reduce the proteins. The sample was then loaded onto a 10 kDa filter unit, and washed three times with 400 μ L 100 mM ammonium bicarbonate at 14,000 g for 15 min. Then 200 μ L of 100-mM ammonium bicarbonate with trypsin at the enzyme-to-protein ratio of 1:100 were added and incubated at 37°C for 20 h. The peptides were harvested by centrifugation, and subsequently dried in a refrigerated CentriVap concentrator (Labconco, Kansas, MO). The tryptic digested peptides were desalted with stage tip C18.

The dried peptides were constituted in 0.1% (v/v) formic acid (FA) solution and analyzed on a Q Exactive Plus mass spectrometer (Thermo Electron Finnigan, San Jose, CA). The peptides were separated on Easynano1200 LC (Thermo, San Jose, CA) equipped with a 150 mm in-house C18 analytical column. The peptides were loaded for 10 min at 3 μ L/min on the trap column in 0.1% FA, then eluted to the analytical column and separated with the following conditions at 300 nL/min, 90 min run with a liquid gradient from 5-90% of solvent B (80% acetonitrile/0.1% FA). The parameters for a full MS survey scan were set at a resolution of 70,000 at 400 m/z over the m/z range of 300-1800, automatic gain controls (AGC) target of $3e6$, maximum ion injection time (IT) of 30 ms. The top 20 multiple-charged parent ions were selected by data dependent MS/MS mode, fragmented by the higher-energy collision dissociation (HCD) with the normalized collision energy of 30% at the m/z scan range of 200-2000. For the MS/MS detection, the resolution was set at 17,500, AGC target value was $2e5$, and the maximum IT was 60 ms. Dynamic exclusion was enabled for 30 s.

The mass spectra were submitted to PD software (Thermo, version 2.2) for peptide identification, and searched against the *Arabidopsis* protein sequences (TAIR9) downloaded from the TAIR website (<http://www.arabidopsis.org/>). The following parameters were used: carbamidomethylation of Cys was set as a fixed modification, oxidation of Met and acetylation of protein N terminal were set as variable modifications, and a maximum of two missed cleavage was allowed.

Co-immunoprecipitation assay

Protoplasts were isolated from leaves of four-week-old *Arabidopsis* plants. Constructs were transformed into the protoplasts and incubated at 22°C in the dark for 12 - 18 h. For heat treatment, the petri dish was incubated in 37°C water bath for 30 min and protoplasts collected into a 1.5 ml Eppendorf by centrifugation at $300 \times g$ for 2 min. After removing the supernatant, protoplasts were lysed with 1 ml of IP buffer (200 mM Tris (pH 9.0), 110 mM potassium acetate, 0.5% Triton-X100, 0.1% Tween-20, 1% protease inhibitor cocktail (Roche), 5 mM DTT). Then the lysate was incubated with 10 μ L IP buffer-balanced GFP-Trap Magnetic Beads at 4°C for 3 hours. The GFP-Trap beads were then magnetically collected and were washed with 1 mL IP buffer for 5 min for 5 times at 4°C. Finally, immunoprecipitated protein complexes were diluted in 5× SDS loading buffer, followed by immunoblotting.

RNA-immunoprecipitation (RIP) sequencing and data analyses

The immunoprecipitation was performed using samples from AP as the previous section described. RNA was extracted using TRIzol (Invitrogen, Cat. No. 15596026) from an aliquot of the AP sample and treated with DNase I (Ambion, Cat. No. AM2222) to eliminate genomic DNA according to manufacturers' guidelines. The RNA was dissolved with 20 μ L RNase-free water. Library preparation was performed at the Genomics Facility of Shanghai Center for Plant Stress Biology. The eluted RNA was used for library preparation

using the NEBNext Ultra II Directional RNA Library Prep Kit (New England BioLabs, Cat. No. E7760) eliminating the mRNA enrichment step. Sequencing was performed on an Illumina NovaSeq 6000 system in the PE150 (pair-end 150 bp) mode.

For RIP-seq data analyses, low-quality and adapter sequences were trimmed from the raw reads using Trim galore v0.4.4_dev with the argument `-q 20`. Then the clean reads were mapped to the *Arabidopsis* reference genome (TAIR10) using STAR v2.6.0a with default parameters except that reads mapped to multiple locations were filtered out with the parameter `'-outFilterMultimapNmax 1'`. BAM files with R1 reads that do not overlap with rRNA annotations were generated using SAMtools (version1.7-16-g5231e3) and were transformed into BED files with BEDtools (v2.27.1-1-gb87c465-dirty). The BED-format alignment data was used as input for Piranha (v1.2.1) peak caller with the parameters `"-z 50 -s -v"` and the 35S::*GFP* sample as a covariant. Peaks with adjusted p-values smaller than 0.01 were then annotated using an in-house script.

Gene IDs of RBGD2/4-associated transcripts were submitted to clueGO (version 2.5.5, Cytoscape plug-in) for gene ontology (GO) analysis using *Arabidopsis thaliana* TAIR10 annotation as the background. The following parameters were used: "Analysis mode" was set as Functional Analysis; "Visual groups" was set as "Groups"; only "Biological Process" was selected in the "ontologies"; "Use GO Term Fusion" was set as TRUE; P-value cut-off was set as 0.01; "GO Tree Interval" was set between 3 and 6; GO term connection cut-off was set as "Kappa Score ≥ 0.25 "; p-value was calculated based on the two-sided hypergeometric test and corrected using the Benjamini-Hochberg method; the "Leading Group Term" was based on the highest-significance; the "Initial Group Size" was set as 1; "% Genes for group merge" was set at 50; "% Terms for group merge" was set at 50.

QUANTIFICATION AND STATISTICAL ANALYSIS

Statistical parameters including the definitions and exact values of n (e.g., number of biological repeats, number of plants, number of cells, etc), distributions and deviations are reported in the Figures and corresponding Figure Legends. $p > 0.05$, not significant, $*p < 0.05$, $**p < 0.01$ by Student's t test, performed in the GraphPad Prism software following standard procedures. Statistical analyses involving high throughput sequencing data were performed in R as described in previous sections.